

Mining Seasonal Temporal Patterns in Big Time Series

Van Long Ho, Nguyen Ho, Torben Bach Pedersen
Aalborg University, Denmark
{vlh,ntth,tbp}@cs.aau.dk

ABSTRACT

Very large time series are increasingly available from an ever wider range of IoT-enabled sensors, from which significant insights can be obtained through mining temporal patterns from them. A useful type of patterns found in many real-world applications exhibit periodic occurrences, and is thus called *seasonal temporal patterns* (STP). Compared to regular patterns, mining seasonal temporal patterns is more challenging since traditional measures such as *support* and *confidence* do not capture the seasonality characteristics. Further, the anti-monotonicity property does not hold for STPs, and thus, resulting in an exponential search space. This paper presents our Frequent Seasonal Temporal Pattern Mining from Time Series (FreqSTPfTS) solution providing: (1) The first solution for seasonal temporal pattern mining (STPM) from time series that can mine STP at different data granularities. (2) The STPM algorithm that uses efficient data structures and two pruning techniques to reduce the search space and speed up the mining process. (3) An approximate version of STPM that uses mutual information, a measure of data correlation, to prune unpromising time series from the search space. (4) An extensive experimental evaluation showing that STPM outperforms the baseline in runtime and memory consumption, and can scale to big datasets. The approximate STPM is up to an order of magnitude faster and less memory consuming than the baseline, while maintaining high accuracy.

1 INTRODUCTION

The widespread of IoT systems enables the collection of big time series from domains such as energy, transportation, climate, and healthcare. Mining such big time series can discover hidden patterns and offer new insights into the application domains to support evidence-based decision making and planning. Often, pattern mining methods such as sequential pattern mining (SPM) [13, 19] and temporal pattern mining (TPM) [11, 20] are used to extract frequent (temporal) relations between events. In SPM, events occur in sequential order, whereas in TPM, events carry additional temporal information such as occurrence time, making relations between temporal events are more expressive and comprehensive. A useful type of temporal patterns found in many real-world applications are those that exhibit periodic occurrences. Such patterns occur concentrated within a particular time period, and then repeat that concentrated occurrence periodically. They are thus called *seasonal temporal patterns*. Here, the term *seasonal* indicates the periodic re-occurrence, while the term *temporal pattern* indicates patterns that are formed by the temporal relations between events, such as follows, contains, overlaps. Seasonal temporal patterns are useful in revealing seasonal information of temporal events and their relations. For example, in healthcare, health experts might be interested in finding seasonal diseases in a geographical location, as shown in Fig. 1. Here, a seasonal temporal pattern involving weather and epidemic events can be found: {Low Temperature overlaps High

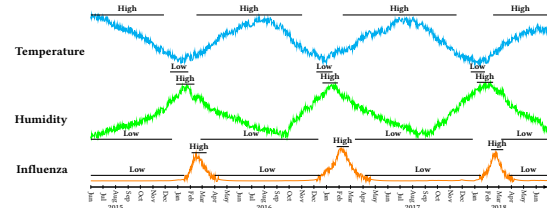


Figure 1: Weather and Influenza time series

Humidity followed by High Influenza Cases}. This pattern occurs yearly and is concentrated in January, February, and March. Detecting such seasonal diseases will support health experts in prevention and planning. In market analysis, knowing the periodic rise of certain stocks and their relations to other impact factors can be of interests for traders to plan better trading strategies. In marketing, identifying the order of search keywords that appear seasonally in the search engine can be useful to better understand customer needs and thereby improve the marketing plans.

Challenges. Although seasonal temporal patterns are useful, mining them is a challenging task for several reasons. First, the *support* measure used by TPM is not sufficient to mine seasonal patterns, since the traditional *support* represents the frequency of a pattern across the entire dataset, and thus, cannot capture the seasonality characteristic of seasonal patterns. Second, since temporal patterns are constructed based on temporal events, the complex relations between temporal events create an exponential and large search space of size $O(n^h 3^{h^2})$ (n is the number of events and h is the length of temporal patterns). Finally, since seasonal temporal patterns do not uphold the anti-monotonicity property, i.e., the non-empty subsets of a seasonal temporal pattern may not be seasonal, mining seasonal temporal patterns is more computationally expensive as the typical pruning technique based on anti-monotonicity property cannot be applied. This raises the need for an efficient seasonal temporal pattern mining approach with effective prunings to tackle the exponential search space. Existing work such as [16, 17] proposes solutions to mine seasonal patterns between itemsets. However, they do not consider the temporal aspect of events, and thus, addressing the exponential search space of seasonal temporal patterns is still an open problem.

Contributions. In the present paper, we present our Frequent Seasonal Temporal Pattern Mining from Big Time Series (FreqSTPfTS) solution that addresses all the above challenges. Specifically, our key contributions are as follows. (1) We propose the first solution to mine *seasonal temporal patterns* from big time series. Within the process, we introduce several measures to assess the seasonality characteristics, and use these to formally define the concept of *seasonal temporal patterns* in time series. The formulation allows to flexibly mine seasonal temporal patterns at different granularities. (2) Our Seasonal Temporal Pattern Mining (STPM) algorithm is efficient and has several important novelties. First, STPM employs efficient data structures, i.e., the hierarchical hash tables, to enable

fast retrieval of candidate events and patterns during the mining process. Second, we define a new measure *maxSeason* that upholds the anti-monotonicity property, and use it to design two efficient pruning techniques: Apriori-like pruning and transitivity pruning. (3) Based on mutual information, we propose a novel approximate version of STPM that prunes unpromising time series which significantly reduces the search space, while maintaining highly accurate results. The approximate STPM can scale on big datasets, i.e., many time series and many sequences. (4) We perform extensive experimental evaluation on synthetic and real-world datasets from various domains which show that STPM outperforms the baseline in both runtime and memory usage. The approximate STPM achieves up to an order of magnitude speedup w.r.t. the baseline, while obtaining high accuracy compared to the exact STPM.

2 RELATED WORK

Seasonal pattern mining (SPM). Finding seasonal patterns that represent temporal periodicity in time series is an important research topic, and has received substantial attention in the last decades. By considering seasonality as periodic occurrences, different techniques have been proposed to find periodic sub-sequences in time series data. Such techniques, first introduced by Han et al. in [9, 10], and later extended by [22, 23, 32], are called *motif* discovery techniques. However, since motifs are defined as similar time series sub-sequences, motif discovery can only find recurrent sub-sequences rather than periodic temporal patterns.

Another research direction in this area concerns periodic association rules [2, 8, 16–18, 29, 30]. Such techniques can identify seasonal associations between itemsets, for example, market-basket analysis to reveal the seasonal occurrence of the association {Glove \Rightarrow Winter Hat} during the winter season. To mine such seasonal itemset patterns in transactional databases, Tanbeer et al. in [29] proposed the PFP-growth algorithm using *minSup* and *maxPer* as seasonality measures. In their method, a tree structure called PF-tree is used as a compact representation of periodic frequent itemsets, with *maxPer* imposing the periodic constraint, and *minSup* imposing the frequency constraint on the pattern occurrences. Although PFP-growth can capture seasonality characteristic through the *maxPer* measure, the use of *minSup* means that it cannot identify rare seasonal patterns. Follow-up work such as [2, 30] improves different aspects of PFP-growth, for example, Amphawan et al. [2] propose *period summary* to approximate the pattern periodicity to reduce the memory cost, Uday et al. [30] propose the concept of *item-specific support* to address the rare pattern problem.

In a more recent work [17], Uday et al. propose the RP-growth algorithm to discover recurring itemset patterns in transactional databases. RP-growth uses an RP-tree to maintain frequent itemsets, and recursively mines the RP-tree to discover recurring patterns. Moreover, RP-growth proposes *recurrence*, a new measure to determine the number of interesting periodic intervals of a pattern, and thus, can identify both regular and rare patterns. However, RP-growth only finds recurring patterns between itemsets without considering their temporal relations. More recently, the same authors introduce several improvements of [17]. In [15], the authors propose the Periodic-Frequent Pattern-growth++ (PFP-growth++) algorithm that employs two new concepts, *local-periodicity* and *periodicity*, to capture locally optimal and globally optimal solutions

of recurring patterns. This enables 2-phase pruning to improve the runtime efficiency. In [16], the authors extend PFP-growth++ to find periodic spatial patterns in spatio-temporal databases. In [18], PFP-growth++ is extended to find maximal periodic frequent patterns. In [14], they further improve PFP-growth++ to be memory efficient by proposing a concept called *period summary* to effectively summarize the temporal occurrence information of an itemset in a Periodic Summary-tree (PS-tree), and designing Periodic Summary Pattern Growth algorithm (PS-growth) to find all periodic-frequent itemset patterns from PS-tree. Nevertheless, all the mentioned work can only discover seasonal patterns between itemsets.

To the best of our knowledge, no existing work addresses the seasonal temporal pattern mining that finds seasonal occurrences of temporal patterns. In Section 6, we adapt the state-of-the-art method for periodic itemset mining *PS-growth* to mine seasonal temporal patterns, and use it as an experimental baseline.

Temporal pattern mining and mutual information. Several TPM methods such as [4, 25, 26, 28], and most recently [11, 20] have been proposed to mine temporal patterns from time series. However, these techniques do not capture the seasonality characteristic needed for seasonal patterns. Particularly, Ho et al. [11] propose a mutual information-based approximation to speed up TPM, but that is based on the pattern confidence, whereas our approximate STPM is based on the pattern support built upon the *maximum season* measure of seasonal temporal patterns.

3 PRELIMINARIES

3.1 Time Granularity

Definition 3.1 (Time domain) A time domain \mathcal{T} consists of an ordered set of time instants that are isomorphic to the natural numbers. The time instants in \mathcal{T} have a time unit, presenting how they are measured.

As an example, consider a time domain \mathcal{T} consisting of an ordered set of minutes. Here, the time instants minute_1 , minute_2 , etc., are isomorphically mapped to the natural numbers, and are measured in the *Minute* time unit.

Definition 3.2 (Time granularity) Given a time domain \mathcal{T} , a *time granularity* G is a *complete and non-overlapping equal partitioning* of \mathcal{T} , i.e., \mathcal{T} is divided into non-overlapping equal partitions. Each non-empty partition $G_i \in G$ is called a (time) *granule*. The position of a granule G_i in G , denoted as $p(G_i)$, is identified by counting the number of granules which appear before and up to (including) G_i .

Consider the time domain \mathcal{T} in the previous example. Here, \mathcal{T} can have different time granularities such as Minute, 5-Minutes, or even Hour, Day, Year. The Minute granularity consists of a set of Minute granules, each representing one unique minute. Instead, the Hour granularity consists of a set of Hour granules, each representing one hour, and is a collection of 60 Minute granules. The position of granule Minute_2 in the Minute granularity is $p(\text{Minute}_2) = 2$.

Definition 3.3 (Finer time granularity) Consider two time granularities G and H . We say that G is a finer granularity than H if and only if for every granule $H_j \in H$, there exists m adjacent granules $G_{i+1}, \dots, G_{i+m} \in G$ such that $H_j = G_{i+1} \cup \dots \cup G_{i+m}$ where $m \geq 1$. We call G is *m-Finer* than H , denoted as $G \leq_m H$.

In the previous example, we have the Minute granularity is 60-Finer than the Hour granularity.

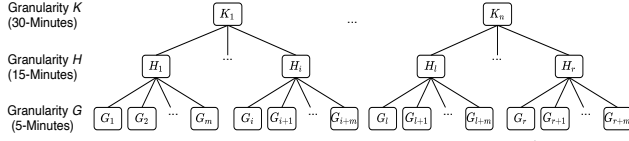


Figure 2: Time granularity hierarchy \mathcal{H}

Definition 3.4 (Time granularity hierarchy) Given a time domain \mathcal{T} , the different time granularities of \mathcal{T} form a *time granularity hierarchy* \mathcal{H} where each level in \mathcal{H} represents one specific granularity, with the lower levels in the hierarchy having finer granularity than the higher levels.

Fig. 2 shows an example of the time granularity hierarchy, where the finest granularity is at the lowest level, and the coarsest granularity is at the highest level in the hierarchy. Here, to be consistent with the examples provided in the following sections, we assume the finest granularity G in Fig. 2 to be 5-Minutes. Thus, the first granule G_1 represents the first 5 minutes of \mathcal{T} , the second granule G_2 represents the second 5 minutes, and so on. Whereas with granularity H , H_1 represents the first 15 minutes of \mathcal{T} , implying that H_1 contains the first three granules G_1, G_2 , and G_3 of G .

Definition 3.5 (Period between two granules) The *period* between two granules G_i and G_j in granularity G measures the time duration between G_i and G_j , and is computed as: $pr_{ij} = |p(G_i) - p(G_j)|$, where $p(G_i)$ and $p(G_j)$ are the positions of G_i and G_j , respectively.

The period between the Minute₁ and Minute₆ granules is:

$|p(\text{Minute}_6) - p(\text{Minute}_1)| = 5$, indicating that the time duration between them is 5 minutes. We note that the period is only defined between granules of the same granularity.

3.2 Symbolic Representation of Time Series

Consider the time domain \mathcal{T} . Let \mathcal{H} be the time granularity hierarchy of \mathcal{T} , and G be the finest granularity in \mathcal{H} . The following definitions are defined on \mathcal{T} and \mathcal{H} .

Definition 3.6 (Time series) A *time series* $X = x_1, x_2, \dots, x_n$ in the time domain \mathcal{T} is a sequence of data values that measure the same phenomenon during an observation time period in \mathcal{T} , and are chronologically ordered. We say that X has granularity G if X is sampled at every time instant t_i in \mathcal{T} .

Definition 3.7 (Symbolic time series) Let X be a time series of granularity G . A *symbolic time series* X_S of X encodes the raw values of X into a sequence of symbols using a mapping function $f: X \rightarrow \Sigma_X$ that maps each value $x_i \in X$ into a symbol $\omega \in \Sigma_X$. The finite set of permitted symbols used to encode X is called the *symbol alphabet* of X , denoted as Σ_X . Furthermore, since the mapping function f performs the 1-to-1 mapping from X to X_S , X_S has the same granularity G as X .

For example, let $X = 1.82, 1.25, 0.46, 0.0$ be a time series representing the energy usage of an electrical device recorded every 5 minutes. Using the symbol alphabet $\Sigma_X = \{1, 0\}$, where 1 indicates the device is on (e.g., $x_i \geq 0.5$), and 0 that the device is off ($x_i < 0.5$), the symbolic representation of X is: $X_S = 1, 1, 0, 0$. Both X and X_S have 5-Minutes granularity. The mapping function f can be defined using time series representation techniques such as SAX [21].

Definition 3.8 (Symbolic database) Given a set of time series $\mathcal{X} = \{X_1, \dots, X_n\}$, the set of symbolic representations of the time series in \mathcal{X} forms a *symbolic database* \mathcal{D}_{SYB} .

In \mathcal{D}_{SYB} , every symbolic time series has the same granularity. Hence, the granularity of \mathcal{D}_{SYB} is the granularity of its symbolic series. Table 1 shows an example of the symbolic database \mathcal{D}_{SYB} . There are 6 time series: {C, D, F, K, M, N} (C: Cooker, D: Dish Washer, F: Food Processor, K: Kettle, M: Microwave, N: Nespresso Coffee) representing the energy usage of electrical devices at 5-Minutes granularity. All time series use the same symbol alphabet $\Sigma = \{0, 1\}$.

3.3 Temporal Event and Temporal Relation

Definition 3.9 (Temporal event in a symbolic time series) Consider a symbolic time series X_S of granularity G . A *temporal event* E in X_S is a tuple $E = (\omega, T)$ where $\omega \in \Sigma_X$ is a symbol, and $T = \{[t_{s_i}, t_{e_i}]\}$ is the set of time intervals during which X_S has the value ω . Here, t_{s_i} is the start time, and t_{e_i} is the end time of each time interval.

Instance of a temporal event: The tuple $e = (\omega, [t_{s_i}, t_{e_i}])$ is called an *instance* of the temporal event $E = (\omega, T)$, representing a single occurrence of E during $[t_{s_i}, t_{e_i}]$. We use the notation $E \triangleright e$ to denote that the event E has an instance e .

Consider the symbolic time series C in Table 1. Then $E = (C:1, \{[1, 2], [4, 4], [7, 8], [19, 24], [31, 31], [34, 35], [40, 41]\})$ is an event of C, representing the time intervals during which C is associated with the symbol 1. The tuple $(C:1, [1, 2])$ is an instance of E . Note that for simplicity, we use the granule positions to represent the start and end times of the time intervals, as the granule position allows to trace back the timestamp associated to each granule.

Relations between temporal events: Let E_i and E_j be two temporal events, and $e_i = (\omega_i, [t_{s_i}, t_{e_i}])$, $e_j = (\omega_j, [t_{s_j}, t_{e_j}])$ be their corresponding instances. We rely on the popular Allens relation model [1] to define 3 basic temporal relations: *Follows*, *Contains*, *Overlaps* between E_i and E_j through e_i and e_j . We avoid the exact time mapping problem in Allens relations by adding a tolerance *buffer* ϵ to the relation's endpoints, while ensuring the relations are *mutually exclusive* (proof in the technical report [12]). Table 2 illustrates the 3 relations and their conditions, with $\epsilon \geq 0$ representing the buffer size, and d_o representing the minimal overlapping duration between two event instances in an *Overlaps* relation.

Definition 3.10 (Temporal pattern) Let $\mathfrak{R} = \{\text{Follows}, \text{Contains}, \text{Overlaps}\}$ be the set of temporal relations. A *temporal pattern* $P = \langle (r_{12}, E_1, E_2), \dots, (r_{(n-1)n}, E_{n-1}, E_n) \rangle$ is a list of triples (r_{ij}, E_i, E_j) , each representing a relation $r_{ij} \in \mathfrak{R}$ between two events E_i and E_j .

Note that the relation r_{ij} in each triple is formed using the specific instances of E_i and E_j . A temporal pattern of n events is called an *n-event pattern*. We use $E_i \in P$ to denote that the event E_i occurs in P , and $P_1 \subseteq P$ to say that a pattern P_1 is a sub-pattern of P .

An example of temporal patterns from Fig. 1 is: $P = \langle (\text{Overlaps}, \text{Low Temperature}, \text{High Humidity}), (\text{Follows}, \text{Low Temperature}, \text{High Influenza Cases}), (\text{Follows}, \text{High Humidity}, \text{High Influenza Cases}) \rangle$. Here, P is a 3-event pattern, containing pairwise temporal relations between three events: Low Temperature, High Humidity, and High Influenza Cases.

3.4 Temporal Sequence Database

Definition 3.11 (Sequence mapping) Consider a symbolic time series X_S of granularity G . Let H be a granularity in \mathcal{H} such that $G \triangleleft_m H$. A sequence mapping $g: X_S \rightarrow_m H$ maps m adjacent symbols in X_S into a single granule $H_i \in H$.

Table 1: A Symbolic Database \mathcal{D}_{SYB} (G: 5-Minutes granularity)

Granules in G	G ₁	G ₂	G ₃	G ₄	G ₅	G ₆	G ₇	G ₈	G ₉	G ₁₀	G ₁₁	G ₁₂	G ₁₃	G ₁₄	G ₁₅	G ₁₆	G ₁₇	G ₁₈	G ₁₉	G ₂₀	G ₂₁	G ₂₂	G ₂₃	G ₂₄	G ₂₅	G ₂₆	G ₂₇	G ₂₈	G ₂₉	G ₃₀	G ₃₁	G ₃₂	G ₃₃	G ₃₄	G ₃₅	G ₃₆	G ₃₇	G ₃₈	G ₃₉	G ₄₀	G ₄₁	G ₄₂					
Position	1	2	3	4	5	6	7	8	9	10	11	12	13	14	15	16	17	18	19	20	21	22	23	24	25	26	27	28	29	30	31	32	33	34	35	36	37	38	39	40	41	42					
C	1	1	0	1	0	0	1	1	0	0	0	0	0	0	0	0	0	0	1	1	1	1	1	1	0	0	0	0	0	0	1	0	0	1	1	0	0	0	1	1	0	1	1	0			
D	1	0	0	1	0	0	1	1	0	1	1	0	0	0	0	0	0	0	1	1	1	1	1	1	0	0	0	0	0	0	1	0	0	1	0	0	1	1	0	1	1	0	1	1	0		
F	0	0	1	0	1	1	0	0	1	0	0	1	1	1	1	0	0	0	0	0	0	0	0	0	0	1	1	1	1	1	1	0	0	1	0	0	1	0	0	1	0	0	1	0	0	1	
K	0	0	1	0	1	1	0	0	1	1	1	1	1	1	1	1	1	1	0	0	0	0	0	0	1	1	1	1	1	1	0	0	1	0	0	1	0	1	0	1	0	0	1	0	0	1	
M	1	1	0	1	0	0	1	1	1	1	1	0	1	1	1	1	1	1	0	0	0	1	1	1	1	1	1	1	1	1	1	1	1	0	1	0	1	0	1	1	1	1	1	1	1	0	
N	1	1	0	1	1	1	1	1	1	1	1	0	1	1	1	1	1	1	0	0	0	0	0	0	1	1	1	1	1	1	1	1	1	1	1	1	1	1	1	1	1	1	1	1	0	0	0

Table 2: Temporal Relations between Events

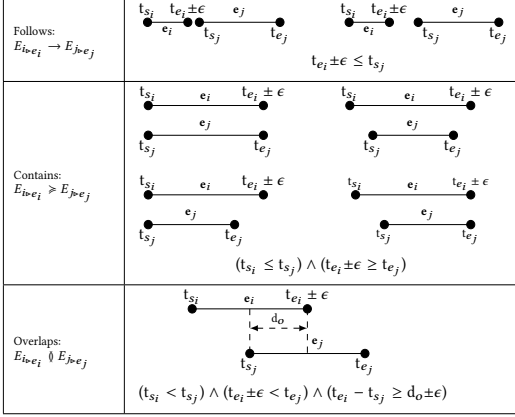


Table 3: A Temporal Sequence Database \mathcal{D}_{SEQ} (H: 15-Minutes granularity)

Granules	Position	Temporal sequences
$H_1 = \{G_1, G_2, G_3\}$	1	(C:1,[1,2]), (C:0,[3,3]), (D:1,[1,1]), (D:0,[2,3]), (F:0,[1,2]), (F:1,[3,3]), (K:0,[1,2]), (K:1,[3,3]), (M:1,[1,2]), (M:0,[3,3]), (N:1,[1,2]), (N:0,[3,3])
$H_2 = \{G_4, G_5, G_6\}$	2	(C:1,[4,4]), (C:0,[5,6]), (D:1,[4,4]), (D:0,[5,6]), (F:0,[4,4]), (F:1,[5,6]), (K:0,[4,4]), (K:1,[5,6]), (M:1,[4,4]), (M:0,[5,6]), (N:1,[4,6]), (N:0,[3,3])
$H_3 = \{G_7, G_8, G_9\}$	3	(C:1,[7,8]), (C:0,[9,9]), (D:1,[7,8]), (D:0,[9,9]), (F:0,[7,8]), (F:1,[9,9]), (K:0,[7,8]), (K:1,[9,9]), (M:1,[7,9]), (N:1,[7,9])
$H_4 = \{G_{10}, G_{11}, G_{12}\}$	4	(C:0,[10,12]), (D:1,[10,11]), (D:0,[12,12]), (F:0,[10,11]), (F:1,[12,12]), (K:1,[10,12]), (M:1,[10,11]), (M:0,[12,12]), (N:1,[10,11]), (N:0,[12,12])
$H_5 = \{G_{13}, G_{14}, G_{15}\}$	5	(C:0,[13,15]), (D:0,[13,15]), (F:1,[13,15]), (K:1,[13,15]), (M:1,[13,15]), (N:1,[13,15])
$H_6 = \{G_{16}, G_{17}, G_{18}\}$	6	(C:0,[16,18]), (D:0,[16,18]), (F:0,[16,18]), (K:1,[16,18]), (M:1,[16,18]), (N:1,[16,18])
$H_7 = \{G_{19}, G_{20}, G_{21}\}$	7	(C:1,[19,21]), (D:1,[19,21]), (F:0,[19,21]), (K:0,[19,21]), (M:0,[19,21]), (N:0,[19,21])
$H_8 = \{G_{22}, G_{23}, G_{24}\}$	8	(C:1,[22,24]), (D:1,[22,24]), (F:0,[22,24]), (K:0,[22,24]), (M:1,[22,24]), (N:0,[22,24])
$H_9 = \{G_{25}, G_{26}, G_{27}\}$	9	(C:0,[25,27]), (D:0,[25,27]), (F:1,[25,27]), (K:1,[25,27]), (M:1,[25,27]), (N:1,[25,27])
$H_{10} = \{G_{28}, G_{29}, G_{30}\}$	10	(C:0,[28,30]), (D:0,[28,30]), (F:1,[28,30]), (K:1,[28,30]), (M:1,[28,30]), (N:1,[28,30])
$H_{11} = \{G_{31}, G_{32}, G_{33}\}$	11	(C:1,[31,31]), (C:0,[32,33]), (D:1,[31,31]), (D:0,[32,33]), (F:0,[31,32]), (F:1,[33,33]), (K:0,[31,32]), (K:1,[33,33]), (M:1,[31,33]), (N:1,[31,33])
$H_{12} = \{G_{34}, G_{35}, G_{36}\}$	12	(C:1,[34,35]), (C:0,[36,36]), (D:1,[34,34]), (D:0,[35,36]), (F:0,[34,35]), (F:1,[36,36]), (K:0,[34,35]), (K:1,[36,36]), (M:0,[34,34]), (M:1,[35,35]), (M:0,[36,36]), (N:1,[34,36])
$H_{13} = \{G_{37}, G_{38}, G_{39}\}$	13	(C:0,[37,39]), (D:1,[37,38]), (D:0,[39,39]), (F:0,[37,38]), (F:1,[39,39]), (K:0,[37,37]), (K:1,[38,39]), (M:1,[37,39]), (N:1,[37,39])
$H_{14} = \{G_{40}, G_{41}, G_{42}\}$	14	(C:1,[40,41]), (C:0,[42,42]), (D:1,[40,41]), (D:0,[42,42]), (F:0,[40,41]), (F:1,[42,42]), (K:0,[40,41]), (K:1,[42,42]), (M:1,[40,42]), (N:0,[40,42])

For example, consider the symbolic time series C in Table 1. Using $G \triangleleft_3 H$, a sequence mapping $g: C \rightarrow_3 H$ maps 3 adjacent symbols of C into one granule H_i in H. After the mapping, we obtain the sequence of symbols for each granule in H as: $H_1: \langle C:1, C:1, C:0 \rangle$, $H_2: \langle C:1, C:0, C:0 \rangle$, $H_3: \langle C:1, C:1, C:0 \rangle$, and so on.

Definition 3.12 (Temporal sequence of a symbolic time series) Consider a symbolic time series X_S of granularity G. Let $\langle \omega_1, \dots, \omega_m \rangle$ be a symbolic sequence at granule H_i in H, obtained by performing a sequence mapping $g: X_S \rightarrow_m H$. A temporal sequence $Seq_i = \langle e_1, \dots, e_n \rangle$ is a list of n event instances, each is obtained by grouping consecutive and identical symbols ω in H_i into an event instance $e = (\omega, [t_s, t_e])$. We say that Seq_i has size n, denoted as $|Seq_i| = n$.

In the previous example, we obtain the temporal sequences for the granules in H as: $Seq_1 = \langle (C:1, [1, 2]), (C:0, [3, 3]) \rangle$, $Seq_2 = \langle (C:1, [4, 4]), (C:0, [5, 6]) \rangle$, $Seq_3 = \langle (C:1, [7, 8]), (C:0, [9, 9]) \rangle$, etc.

Definition 3.13 (Temporal sequence database) Consider a symbolic database \mathcal{D}_{SYB} of granularity G (defined in Def 3.8) which contains a collection of symbolic time series $\{X_S\}$, and a granularity $H \in \mathcal{H}$. Let $g: X_S \rightarrow_m H$ be a sequence mapping applied to each symbolic time series X_S in \mathcal{D}_{SYB} . The temporal sequences obtained from this mapping form a temporal sequence database \mathcal{D}_{SEQ} where each row is a set of sequences $\{Seq_i\}$ that belong to the same granule $H_i \in \mathcal{H}$. The temporal sequence database \mathcal{D}_{SEQ} has granularity H.

Table 3 shows an example of \mathcal{D}_{SEQ} , obtained from \mathcal{D}_{SYB} in Table 1 using the mapping $g: X_S \rightarrow_3 H$ on the six symbolic time series $\{C, D, F, K, M, N\}$. Each row i in Table 3 contains the temporal sequences of $\{C, D, F, K, M, N\}$ belonging to the same granule H_i . For instance, row 1 includes the sequences of the six symbolic series at the first granule $H_1 = \{G_1, G_2, G_3\}$: $Seq_{H_1} = \langle (C:1, [1, 2]), (C:0, [3, 3]), (D:1, [1, 1]), (D:0, [2, 3]), (F:0, [1, 2]), (F:1, [3, 3]), (K:0, [1, 2]), (K:1, [3, 3]), (M:1, [1, 2]), (M:0, [3, 3]), (N:1, [1, 2]), (N:0, [3, 3]) \rangle$. Furthermore, since G is a 5-Minutes granularity, H is a 15-Minutes granularity.

Given a symbolic database \mathcal{D}_{SYB} of granularity G, and a granularity hierarchy \mathcal{H} , we can construct different temporal sequence databases \mathcal{D}_{SEQ} of different granularities $H \in \mathcal{H}$ by using different sequence mappings $g: X_S \rightarrow_m H$. For instance, in the previous

example, using $g: X_S \rightarrow_3 H$, we obtain \mathcal{D}_{SEQ} at 15-Minutes granularity. Using $g: X_S \rightarrow_{12} H$, we obtain \mathcal{D}_{SEQ} at 1-Hour granularity.

Definition 3.14 (Temporal sequence supporting a temporal pattern) Let $Seq_k = \langle e_1, \dots, e_n \rangle$ be a temporal sequence at granule H_k in \mathcal{D}_{SEQ} . We say that Seq_k supports a temporal pattern P, denoted as $P \in Seq_k$, iff $|Seq_k| \geq 2 \wedge \forall (r_{ij}, E_i, E_j) \in P: \exists (e_l, e_m) \in Seq_k$ such that r_{ij} holds between $E_{i \triangleright e_l}$ and $E_{j \triangleright e_m}$. Furthermore, the granule H_k in which pattern P occurs is denoted as H_k^P .

In Def 3.14, a sequence Seq_k supports a pattern P if every relation r_{ij} in P is formed through a pair of event instances (e_l, e_m) in Seq_k . In Table 3, consider the sequence $Seq_1 = \langle e_1 = (C:1, [1, 2]), e_2 = (C:0, [3, 3]), e_3 = (D:1, [1, 1]), \dots, e_{11} = (N:1, [1, 2]), e_{12} = (N:0, [3, 3]) \rangle$ at granule H_1 . Here, Seq_1 supports a 3-event pattern $P = \langle (\text{Follows}, C:1 \triangleright e_1, C:0 \triangleright e_2), (\text{Contains}, C:1 \triangleright e_1, D:1 \triangleright e_3), (\text{Follows}, D:1 \triangleright e_3, C:0 \triangleright e_2) \rangle$ through the first three instances e_1, e_2 , and e_3 .

3.5 Frequent Seasonal Temporal Pattern

Definition 3.15 (Support set of a temporal event) Consider a temporal sequence database \mathcal{D}_{SEQ} of granularity H, and a temporal event E. The set of granules H_i in \mathcal{D}_{SEQ} where E occurs, arranged in an increasing order, is called the support set of event E, and is denoted as $\text{SUP}^E = \{H_1^E, \dots, H_r^E\}$, with $1 \leq l \leq r \leq |\mathcal{D}_{\text{SEQ}}|$.

The support set of a group of events (E_i, \dots, E_k) : is the set of granules H_i in \mathcal{D}_{SEQ} where (E_i, \dots, E_k) concurrently occur, and is denoted as $\text{SUP}^{(E_i, \dots, E_k)}$.

The support set of a temporal pattern: Consider a temporal sequence database \mathcal{D}_{SEQ} of granularity H, and a temporal pattern P. The set of granules H_i in \mathcal{D}_{SEQ} where P occurs, arranged in an increasing order, is called the support set of pattern P, and is denoted as $\text{SUP}^P = \{H_1^P, \dots, H_r^P\}$, with $1 \leq l \leq r \leq |\mathcal{D}_{\text{SEQ}}|$.

Definition 3.16 (Near support set of a temporal pattern) Consider a pattern P with the support set $\text{SUP}^P = \{H_1^P, \dots, H_r^P\}$. Let maxPeriod be the maximum period threshold, representing the predefined maximal period between any two consecutive granules in SUP^P . Further, let $\text{sup}^P = \{H_m^P, \dots, H_q^P\} \subseteq \text{SUP}^P$ be a subset of SUP^P . The set sup^P is called a near support set of P if $\forall (H_o^P, H_p^P) \in \text{sup}^P$:

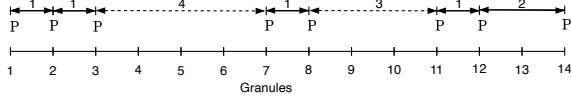


Figure 3: Near support sets of pattern $P = C:1 \geq D:1$

(H_o^P and H_p^P are consecutive) $\wedge |p(H_o^P) - p(H_p^P)| \leq \text{maxPeriod}$, where $p(H_o^P)$ and $p(H_p^P)$ are the positions of H_o^P and H_p^P in granularity H . We denote the near support set of pattern P as NearSUP^P .

We note that the term *near support set* is inspired by the mathematical concept called *near set* [3] which represents a set whose elements are either spatially or descriptively close. In our context, the near support set of P is a support set where P 's occurrences are close in time, i.e., any two consecutive occurrences of P have to be within the maximal period maxPeriod . Moreover, NearSUP^P is called a *maximal near support set* if NearSUP^P has no other superset beside itself which is also a near support set.

As an example, consider the pattern $P = (\text{Contains}, C:1, D:1)$ (or $C:1 \geq D:1$) in Table 3, and let $\text{maxPeriod} = 2$. Here, the support set of P is $\text{SUP}^P = \{1, 2, 3, 7, 8, 11, 12, 14\}$. Hence, P has three maximal near support sets: $\text{NearSUP}_1^P = \{1, 2, 3\}$, $\text{NearSUP}_2^P = \{7, 8\}$, and $\text{NearSUP}_3^P = \{11, 12, 14\}$, since the periods between any two consecutive granules in the three sets are less than or equal to maxPeriod . Fig. 3 illustrates the three near support sets of P .

Definition 3.17 (Season of a temporal pattern) Let NearSUP^P be a near support set of a pattern P . Then NearSUP^P is called a *season* of P if $\text{den}(\text{NearSUP}^P) = |\text{NearSUP}^P| \geq \text{minDensity}$, where $\text{den}(\text{NearSUP}^P)$ computes the *density of the near support set* NearSUP^P , representing the number of granules that supports P , and minDensity is a predefined minimum density threshold.

The density of a near support set measures how dense a near support set of the pattern P is. The higher the density, the more occurrences of P appear in the set. For instance, in the previous example, we have $\text{den}(\text{NearSUP}_1^P) = |\text{NearSUP}_1^P| = 3$. Similarly, $\text{den}(\text{NearSUP}_2^P) = 2$, $\text{den}(\text{NearSUP}_3^P) = 3$. If the occurrences of a pattern P are dense enough, the near support set becomes a season of P . Intuitively, a *season* of a temporal pattern is a *concentrated time period* in which the pattern *occurs one or more times*, separated by a longer *gap period* of no occurrences, before the next season starts in a periodic fashion.

Definition 3.18 (Distance between two seasons) Let $\text{NearSUP}_i^P = \{H_k^P, \dots, H_n^P\}$ and $\text{NearSUP}_j^P = \{H_r^P, \dots, H_u^P\}$ be two seasons of a pattern P where $n < r$. The *distance* between NearSUP_i^P and NearSUP_j^P is the period between the last granule H_n^P in NearSUP_i^P and the first granule H_r^P in NearSUP_j^P , and is computed as: $\text{dist}(\text{NearSUP}_i^P, \text{NearSUP}_j^P) = |p(H_n^P) - p(H_r^P)|$.

The distance measure shows how far two seasons of a pattern P are from each other. For instance, in Fig. 3, the distance between NearSUP_1^P and NearSUP_2^P is 4, and between NearSUP_2^P and NearSUP_3^P is 3. Based on the season concept and the distance measure, we define a frequent seasonal temporal pattern as follows.

Definition 3.19 (Frequent seasonal temporal pattern) Consider a temporal pattern P . Let $\mathcal{PS} = \{\text{NearSUP}^P\}$ be the set of seasons of P , and minSeason be the *minimum seasonal occurrence threshold*, $\text{distInterval} = [\text{dist}_{\min}, \text{dist}_{\max}]$ be the *distance interval* where dist_{\min} is the minimum distance, and dist_{\max} is the

maximum distance. A temporal pattern P is called a *frequent seasonal temporal pattern* iff $\text{seasons}(P) = |\mathcal{PS}| \geq \text{minSeason} \wedge \forall (\text{NearSUP}_i^P, \text{NearSUP}_j^P) \in \mathcal{PS}$: they are consecutive seasons and $\text{dist}_{\min} \leq \text{dist}(\text{NearSUP}_i^P, \text{NearSUP}_j^P) \leq \text{dist}_{\max}$.

Intuitively, a pattern P is seasonal if the distance between two consecutive seasons is within the predefined distance interval. Moreover, a seasonal temporal pattern is frequent if it occurs more often than a predefined *minimum seasonal occurrence threshold* minSeason . The number of seasons of a pattern P is the size of \mathcal{PS} , and is computed as $\text{seasons}(P) = |\mathcal{PS}|$.

Mining Frequent Seasonal Temporal Patterns from Time Series (FreqSTPfts). Given a set of n time series $\mathcal{X} = \{X_1, \dots, X_n\}$ of granularity G , let \mathcal{D}_{SEQ} be the temporal sequence database of granularity $H \in \mathcal{H}$ obtained from \mathcal{X} , and maxPeriod , minDensity , distInterval , and minSeason be the maximum period, minimum density, distance interval, and minimum seasonal occurrence thresholds, respectively. The FreqSTPfts problem aims to find all frequent seasonal temporal patterns P in \mathcal{D}_{SEQ} that satisfy the maxPeriod , minDensity , distInterval , and minSeason constraints.

4 FREQUENT SEASONAL TEMPORAL PATTERN MINING

4.1 Overview of FreqSTPfts Mining Process

Fig. 4 gives an overview of the FreqSTPfts mining that consists of two phases. **Phase 1**, *Data Transformation*, converts a set of time series \mathcal{X} into a symbolic database \mathcal{D}_{SYB} (Step 1.1) by using the mapping function defined in Def. 3.7, and then converts \mathcal{D}_{SYB} into a temporal sequence database \mathcal{D}_{SEQ} (Step 1.2) by applying the sequence mapping defined in Def. 3.11 to map m adjacent symbols of granularity G in \mathcal{D}_{SYB} into a temporal sequence of granularity H , with $G \triangleleft_m H$. **Phase 2**, *Seasonal Temporal Pattern Mining (STPM)*, mines frequent seasonal temporal patterns and consists of two steps: (Step 2.1) *Seasonal Single Event Mining*, and (Step 2.2) *Seasonal k-Event Pattern Mining* ($k \geq 2$). The final output of STPM is the set of all frequent seasonal temporal patterns in \mathcal{D}_{SEQ} .

Before introducing the STPM algorithm in detail, we first present the concept of *candidate seasonal pattern*, which is designed to support Apriori-like pruning in STPM.

4.2 Candidate Seasonal Pattern

Pattern mining methods often use the *anti-monotonicity* property of the *support* measure to reduce the search space [25]. Specifically, this property ensures that an infrequent event A cannot generate a frequent event pair (A, B) , since $\text{support}(A) \geq \text{support}(A, B)$. Hence, if A is infrequent, we can safely remove A and any of its combinations from the search space, and the algorithm completeness is still guaranteed. However, seasonal temporal patterns constrained by the maxPeriod , minDensity , distInterval and minSeason thresholds do *not* uphold this property, as illustrated below.

Consider a 1-event pattern (called a single event) $P_1 = M:1$, and a 2-event pattern $P_2 = M:1 \geq N:1$, in Table 3. Let $\text{maxPeriod} = 2$, $\text{minDensity} = 3$, $\text{distInterval} = [4, 10]$, and $\text{minSeason} = 2$. From the constraints, we can identify the seasons of P_1 and P_2 , respectively, as: $\mathcal{PS}^{P_1} = \{\text{NearSUP}_1^{P_1} = \{1, 2, 3, 4, 5, 6, 8, 9, 10, 11, 12, 13, 14\}\}$ and $\mathcal{PS}^{P_2} = \{\text{NearSUP}_1^{P_2} = \{1, 3, 4, 5, 6\}, \text{NearSUP}_2^{P_2} = \{10, 11, 13\}\}$. Hence, we have: $|\mathcal{PS}^{P_1}| = 1$ and $|\mathcal{PS}^{P_2}| = 2$. Due to the minSeason constraint, P_1 is not a frequent seasonal pattern, whereas

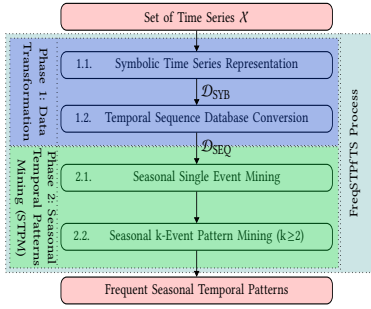


Figure 4: The FreqSTPfTS process

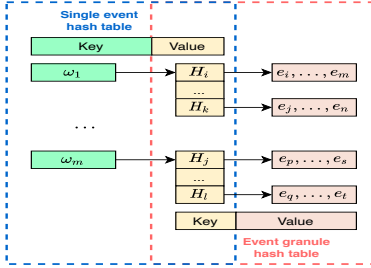


Figure 5: The HLL_1 structure

P_2 is. Because P_1 is a sub-pattern of P_2 , this shows that seasonal temporal patterns do not adhere to the anti-monotonic property.

However, to improve STPM performance, it is necessary to reduce its search space. For this reason, we propose the *maximum seasonal occurrence* measure, called *maxSeason*, that upholds the anti-monotonicity property to prune infrequent patterns. The *maxSeason* is indeed an upper bound on the seasons of a pattern. **Maximum seasonal occurrence of a single event E** : is the ratio between the number of granules in the support set SUP^E of E in \mathcal{D}_{SEQ} , and the *minDensity* threshold:

$$maxSeason(E) = \frac{|SUP^E|}{minDensity} \quad (1)$$

Eq. (1) divides the number of granules containing E by the minimum density of a season. Thus, it computes the maximum seasons a single event E can have, given \mathcal{D}_{SEQ} . Similarly, the maximum seasonal occurrence of a group of events (E_i, \dots, E_k) , denoted as $maxSeason(E_i, \dots, E_k)$, is the ratio between the number of granules in the support set of (E_i, \dots, E_k) and the *minDensity*.

Maximum seasonal occurrence of a temporal pattern P : is the ratio between the number of granules in the support set SUP^P of P , and the *minDensity* threshold:

$$maxSeason(P) = \frac{|SUP^P|}{minDensity} \quad (2)$$

The *maxSeason* upholds anti-monotonicity property, shown below.

LEMMA 1. Let G_E be a group of temporal events, and G'_E be a subset of G_E , i.e., $G'_E \subseteq G_E$. Then $maxSeason(G'_E) \geq maxSeason(G_E)$.

LEMMA 2. Let P be a temporal pattern, and P' be a sub-pattern of P , i.e., $P' \subseteq P$. Then $maxSeason(P') \geq maxSeason(P)$.

PROOF. Detailed proofs of all lemmas, theorems, and complexities in this article can be found in the technical report [12]. \square

From Lemmas 1 and 2, the *maxSeason* of a group of events G_E (or pattern P) is always at most the *maxSeason* of its subset G'_E (or sub-pattern P'). Thus, *maxSeason* upholds the anti-monotonicity property, and can be used to reduce the search space of STPM. Below,

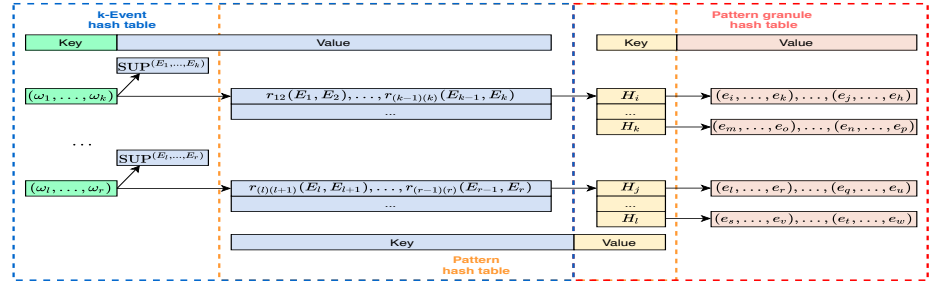


Figure 6: The HLL_k ($k \geq 2$) structure

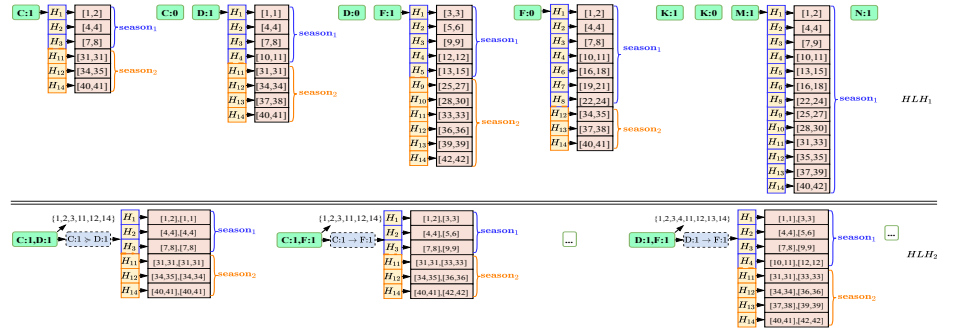


Figure 7: A Hierarchical Pattern Graph for Table 3

we define the *candidate pattern* concept that uses *maxSeason* as a gatekeeper to identify frequent/ infrequent seasonal patterns.

Candidate seasonal pattern: A temporal pattern P is a *candidate seasonal pattern* if $maxSeason(P) \geq minSeason$.

Similarly, a group of k events $G_E = (E_1, \dots, E_k)$ ($k \geq 1$) is a *candidate seasonal k -event group* if $maxSeason(G_E) \geq minSeason$. Intuitively, a pattern P (or k -event group G_E) can potentially be frequent if its *maxSeason* is greater than the predefined minimum seasonal occurrence threshold *minSeason*. In contrast, a pattern P (or G_E) cannot be frequent if its *maxSeason* is less than *minSeason*. Hence, P can be safely removed from the search space.

Next, we present our STPM algorithm, and discuss in details the two mining steps. Algorithm 1 provides the pseudo-code of STPM.

4.3 Mining Seasonal Single Events

The first step in STPM is to mine frequent seasonal single events (Alg. 1, lines 1-9) that satisfy the constraints *maxPeriod*, *minDensity*, *distInterval* and *minSeason*. To do that, we first look for the candidate seasonal single events defined in Section 4.2, and then use only the found candidates to mine frequent seasonal events.

The candidate seasonal events are found by first scanning \mathcal{D}_{SEQ} to identify the support set SUP^{E_i} for each event E_i . Given the found support set SUP^{E_i} and the *minDensity* threshold, we compute the maximum seasonal occurrence $maxSeason(E_i)$ for event E_i . If the computed $maxSeason(E_i) \geq minSeason$, then E_i is a candidate seasonal event. Otherwise, E_i is not a candidate and is removed from the search space. Note that we only need to scan \mathcal{D}_{SEQ} once to find all candidate seasonal events.

We use the found candidate events to mine frequent seasonal events. For each candidate E_i , we iterate through the support set SUP^{E_i} , and calculate the period pr_{ij} between every two consecutive granules in SUP^{E_i} , and determine the near support sets $NearSUP^{E_i}$ that satisfy *maxPeriod* and *minDensity*. Next, the set of seasons $\mathcal{P}S^{E_i}$ is identified by selecting the near support sets that adhere to *distInterval*. Finally, the frequent seasonal single events are

determined by comparing the number of seasons of E_i to $minSeason$, selecting only those that have $seasons(E_i) = |\mathcal{P}S^{E_i}| \geq minSeason$.

We use a *hierarchical lookup hash structure* HLH_1 to store the candidate seasonal single events. This data structure enables fast search when mining seasonal k-events patterns ($k \geq 2$). Note that we maintain the candidate events in HLH_1 instead of the frequent seasonal events, as the $maxSeason$ of candidate events upholds the anti-monotonicity property, and can thus be used for pruning. We illustrate HLH_1 in Fig. 5, and describe the data structure below.

Hierarchical lookup hash structure HLH_1 : The HLH_1 is a hierarchical data structure that consists of two hash tables: the *single event hash table* EH and the *event granule hash table* GH . Each hash table has a list of <key, value> pairs, with the value in EH used as the key in GH . More specifically, the EH table maintains candidate single events found in \mathcal{D}_{SEQ} . For a <key, value> pair in EH , the key is the event symbol $\omega \in \Sigma_X$ representing the candidate seasonal event E_i , and the value is the list of granules $\langle H_1, \dots, H_k \rangle$ in SUP^{E_i} . Instead, the GH table maintains the instances of E_i . The key in GH is the value of EH , i.e., the list of granules, while the value in GH stores event instances of E_i that appear at the corresponding granule in \mathcal{D}_{SEQ} . The HLH_1 data structure enables fast retrieval of event granules and event instances when mining candidate seasonal k-event patterns in the next steps of STPM.

We provide an example of the hierarchical lookup hash structure HLH_1 in Fig. 7 that is built using Table 3 with $maxPeriod = 2$, $minDensity = 3$, $distInterval = [4, 10]$, and $minSeason = 2$. Here, out of 12 events in \mathcal{D}_{SEQ} , we have ten candidate seasonal single events stored in HLH_1 : C:1, C:0, D:1, D:0, F:1, F:0, K:1, K:0, M:1, and N:1. Due to space limitations, we only provide the detailed internal structure of five candidate events in Fig. 7. Among the ten candidate events, the event M:1 does not satisfy the $minSeason$ threshold since $season(M:1) = 1$, and thus, is not a frequent seasonal single event. However, M:1 is still present in HLH_1 as M:1 might create frequent seasonal k-event patterns. In contrast, N:0 and M:0 are not the candidate seasonal single events because they do not satisfy $maxSeason$ constraint, and thus, are omitted from HLH_1 .

Complexity: The complexity of finding frequent seasonal single events is $O(n \cdot |\mathcal{D}_{SEQ}|)$, where n is the number of distinct events.

4.4 Mining Seasonal k-event Patterns

Search space of STPM. The next step of STPM is to mine frequent seasonal k-event patterns ($k \geq 2$). A straightforward approach is to enumerate all possible k-event combinations, and check whether each combination can form frequent seasonal patterns. However, this naive approach is very expensive as it creates a very large search space, approximately of size $O(n^h 3^{h^2})$, where n is the number of distinct events in \mathcal{D}_{SEQ} , and h is the maximal length of a temporal pattern, making it computationally prohibitive to mine seasonal patterns. Detailed derivation and the proof of the search space complexity are provided in [12]. The problem of a large search space is thus alleviated by using an iterative mining process that first finds candidate seasonal k-event groups, and then mines frequent seasonal k-event patterns only from the candidates. Below, we first introduce the data structure used in this mining step.

The hierarchical lookup hash structure HLH_k : Similar to single events, we use the *hierarchical lookup hash structure* HLH_k ($k \geq 2$) to maintain candidate seasonal k-event groups and patterns,

Algorithm 1: Frequent Seasonal Temporal Pattern Mining

Input: Temporal sequence database \mathcal{D}_{SEQ} , the thresholds: $maxPeriod, minDensity, distInterval, minSeason$

Output: The set of frequent seasonal temporal patterns \mathcal{P}

// Step 2.1: Mining frequent seasonal single events

```

1: foreach event  $E_i \in \mathcal{D}_{SEQ}$  do
2:   Find  $SUP^{E_i}$  and compute  $maxSeason(E_i)$ ;
3:   if  $maxSeason(E_i) \geq minSeason$  then
4:     Insert  $E_i$  into  $Candidate1Event$ ;
5: foreach candidate  $E_i \in Candidate1Event$  do
6:   Find  $NearSUP^{E_i}$  that satisfies  $maxPeriod$  and  $minDensity$ ;
7:   Find  $PS^{E_i}$  that adheres  $distInterval$ ;
8:   if  $|PS^{E_i}| \geq minSeason$  then
9:     Insert  $E_i$  into  $\mathcal{P}$ ; //  $E_i$  is a frequent seasonal single event
// Step 2.2: Mining frequent seasonal k-event patterns,  $k \geq 2$ 
10: FilteredF1  $\leftarrow$  Transitivity_Filtering( $F_1$ );
11: kEventGroups  $\leftarrow$  Cartesian(FilteredF1,  $F_{k-1}$ );
12: CandidatekEvent  $\leftarrow$  maxSeason_Filtering(kEventGroups);
13: foreach kEvent in  $CandidatekEvent$  do
14:   (k-1)-event_patterns  $\leftarrow$  Retrieve_Relations( $PH_{k-1}$ );
15:   k-event_patterns  $\leftarrow$  Iterative_Check((k-1)-event_patterns,  $E_k$ );
16:   foreach  $P$  in k-event_patterns do
17:     if  $maxSeason(P) \geq minSeason$  then
18:       Insert  $P$  into  $CandidatekPatterns$ ;
19: foreach candidate  $P \in CandidatekPatterns$  do
20:   Determine  $NearSUP^P$  satisfying  $maxperiod$  and  $minDensity$ ;
21:   Identify  $\mathcal{P}S^P$  adhering to  $distInterval$ ;
22:   if  $|\mathcal{P}S^P| \geq minSeason$  then
23:     Insert  $P$  into  $\mathcal{P}$ ; //  $P$  is a frequent seasonal pattern

```

as illustrated in Fig. 6. The index k in HLH_k denotes the hash structure used at level k of STPM. For example, HLH_2 is used at level 2 for mining seasonal 2-event patterns, and HLH_3 is used for mining 3-event patterns, and so on.

The HLH_k structure contains three hash tables: the *k-event hash table* EH_k , the *pattern hash table* PH_k , and the *pattern granule hash table* GH_k . The EH_k table maintains the information of candidate k-event groups, and their corresponding k-event patterns. Thus, for each <key, value> pair of EH_k , *key* is the list of symbols $(\omega_1, \dots, \omega_k)$ that represent the candidate k-event group (E_1, \dots, E_k) , and *value* is an *object* that consists of two components: (1) the support set $SUP^{(E_1, \dots, E_k)}$, and (2) a list of candidate seasonal k-event temporal patterns $P = \{(r_{12}, E_1, E_2), \dots, (r_{(k-1)(k)}, E_{k-1}, E_k)\}$, created from the k-event group (E_1, \dots, E_k) .

The PH_k table maintains information about candidate k-event patterns and their corresponding granules. As shown in Fig. 6, *key* of PH_k is the candidate pattern P which is indeed the *value* component of EH_k , while *value* of PH_k is the list of granules that contain P . Finally, the GH_k table maintains the event instances involved in pattern P . In the GH_k table, *key* of GH_k is the list of granules containing P , which is indeed the *value* component of PH_k , while *value* of GH_k is the list of event instances from which the temporal relations in P are formed. The HLH_k hash structure helps speed up the candidate seasonal k-event group mining through the use of the support set in EH_k , and enables fast search for temporal relations between k events using the information in PH_k and GH_k .

4.4.1 Mining candidate seasonal k-event groups. STPM uses the anti-monotonicity property of the $maxSeason$ to find candidate seasonal k-event groups.

LEMMA 3. *Let P be a k-event temporal pattern formed by a k-event group (E_1, \dots, E_k) . Then, $maxSeason(P) \leq maxSeason(E_1, \dots, E_k)$.*

From Lemma 3, the maximum seasonal occurrence of a pattern P is at most the maximum seasonal occurrence of its events. Thus, an infrequent k-event group (E_1, \dots, E_k) (i.e., $maxSeason(E_1, \dots, E_k) < minSeason$) cannot form frequent seasonal patterns and thus, can be pruned from the search space. Based on Lemma 3, we mine the candidate seasonal k-event groups as follows (Alg. 1, lines 10-12).

Let F_{k-1} be the set of candidate seasonal (k-1)-event groups found in HLH_{k-1} , and F_1 be the set of candidate seasonal single events in HLH_1 . We first generate all possible k-event groups by computing the Cartesian product $F_{k-1} \times F_1$. Next, for each k-event group (E_1, \dots, E_k) , we compute the support set $SUP^{(E_1, \dots, E_k)}$ by taking the intersection between the support set $SUP^{(E_1, \dots, E_{k-1})}$ of (E_1, \dots, E_{k-1}) in EH_{k-1} , and the support set SUP^{E_k} of E_k in EH . The intersection operation returns a set of granules that contain the k-event group (E_1, \dots, E_k) . Next, given the support set $SUP^{(E_1, \dots, E_k)}$ and the $minDensity$ threshold, we compute the maximum seasonal occurrence $maxSeason(E_1, \dots, E_k)$ using Eq. (1), and evaluate whether (E_1, \dots, E_k) is a candidate k-event group, i.e., $maxSeason(E_1, \dots, E_k) \geq minSeason$. If (E_1, \dots, E_k) is a candidate, it is stored in the EH_k table of HLH_k .

4.4.2 Mining frequent seasonal k-event patterns. We use the found candidate k-event groups to mine frequent seasonal k-event patterns (Alg. 1, lines 13-23). We first discuss the case of 2-event patterns, and then generalize to k-event patterns.

4.4.2.1 Mining frequent seasonal 2-event patterns: We first mine the candidate 2-event patterns. For each candidate 2-event group (E_i, E_j) , we use the support set $SUP^{(E_i, E_j)}$ to retrieve the temporal sequences \mathcal{S} that contain (E_i, E_j) . Next, for each sequence $S \in \mathcal{S}$, we extract their event instances (e_i, e_j) , and verify the relation between them. We then compute the $maxSeason$ of the 2-event pattern P and determine if P is a candidate pattern, i.e., $maxSeason(P) \geq minSeason$. Finally, the candidate seasonal 2-event patterns are stored in PH_2 table, while their event instances are stored in GH_2 table.

Based on the set of candidate seasonal 2-event patterns P , we determine whether P is a frequent seasonal 2-event pattern by checking the constraints of $maxPeriod$, $minDensity$, $distInterval$ and $minSeason$, as in the case of single events, using the support set SUP^P which is the value of PH_2 .

4.4.2.2 Mining frequent seasonal k-event patterns: Mining seasonal k-event patterns is similar to 2-event patterns. Let $N_{k-1} = (E_1, \dots, E_{k-1})$ be a candidate (k-1)-event group in HLH_{k-1} , $N_1 = (E_k)$ be a candidate single event in HLH_1 , and $N_k = N_{k-1} \cup N_1 = (E_1, \dots, E_k)$ be a candidate k-event in HLH_k .

To find k-event patterns for N_k , we first retrieve the set of candidate (k-1)-event patterns \mathcal{P}_{k-1} by accessing the EH_{k-1} table. Each $P_{k-1} \in \mathcal{P}_{k-1}$ is a list of $\frac{1}{2}(k-1)(k-2)$ triples: $\{(r_{12}, E_1, E_2), \dots, (r_{(k-2)(k-1)}, E_{k-2}, E_{k-1})\}$. We iteratively verify the possibility of P_{k-1} forming a k-event pattern P_k with E_k as follows.

We first start with the triple $(r_{(k-1)k}, E_{k-1}, E_k)$. If $(r_{(k-1)k}, E_{k-1}, E_k)$ does not exist in HLH_2 , then P_k is not a candidate k-event pattern, and the verification stops immediately. Otherwise, we compute the support set SUP^{P_k} of the pattern P_k by intersecting $SUP^{P_{k-1}}$ and SUP^{E_k} . We continue the similar verification on the triple $(r_{(k-2)k}, E_{k-2}, E_k)$, until it reaches (r_{1k}, E_1, E_k) . Finally, we compute the maximum seasonal occurrence $maxSeason(P_k)$ using SUP^{P_k} to determine whether P_k is a candidate k-event pattern, i.e., $maxSeason(P_k) \geq minSeason$. The candidate k-event patterns are stored in PH_k and GH_k .

Next, we mine frequent seasonal k-event patterns from the found candidates by checking the constraints $maxPeriod$, $minDensity$, $distInterval$ and $minSeason$, similar to 2-event patterns.

Using transitivity property to optimize candidate k-event groups: In Section 4.4.1, when mining candidate k-event groups, we perform the Cartesian product between F_{k-1} and F_1 . However, using the candidate single events in F_1 to generate k-event groups can create redundancy, since events in F_1 when combined with F_{k-1} might not form any frequent seasonal k-event patterns. For example, consider the event F:0 in HLH_1 in Fig. 7. Here, F:0 is a candidate single event, and thus, can be combined with 2-event groups in HLH_2 such as (C:1, D:1) to create a 3-event group (C:1, D:1, F:0). However, (C:1, D:1, F:0) cannot form any candidate seasonal 3-event patterns, since F:0 is not present in any candidate 2-event patterns in HLH_2 . To reduce such redundancy and further optimize the mining, we use the *transitivity property* of temporal relations to identify such event groups.

LEMMA 4. *Let $S = \langle e_1, \dots, e_{k-1} \rangle$ be a temporal sequence that supports a (k-1)-event pattern $P = \langle (r_{12}, E_{1 \rightarrow e_1}, E_{2 \rightarrow e_2}), \dots, (r_{(k-2)(k-1)}, E_{k-2 \rightarrow e_{k-2}}, E_{k-1 \rightarrow e_{k-1}}) \rangle$. Let e_k be a new event instance added to S to create the temporal sequence $S' = \langle e_1, \dots, e_k \rangle$.*

The set of temporal relations \mathfrak{R} is transitive on S' : $\forall e_i \in S', i < k, \exists r \in \mathfrak{R}$ s.t. $r(E_{i \rightarrow e_i}, E_{k \rightarrow e_k})$ hold.

Lemma 4 states the temporal transitivity property between temporal events, and is used to prove the following lemma.

LEMMA 5. *Let $N_{k-1} = (E_1, \dots, E_{k-1})$ be a candidate seasonal (k-1)-event group, and E_k be a candidate seasonal single event. The group $N_k = N_{k-1} \cup E_k$ can form candidate seasonal k-event temporal patterns if $\forall E_i \in N_{k-1}, \exists r \in \mathfrak{R}$ s.t. $r(E_i, E_k)$ is a candidate seasonal temporal relation.*

From Lemma 5, only single events in HLH_1 that occur in HLH_{k-1} should be used to create k-event groups. We identify these single events by filtering F_1 , and creating the set $FilteredF1$. Then, the Cartesian product $F_{k-1} \times F_1$ is replaced by $F_{k-1} \times FilteredF1$ to generate k-event groups.

Complexity: Let n be the number of single events in HLH_1 , i be the average number of event instances of each event, r be the number of (k-1)-event patterns in HLH_{k-1} , and u be the average number of granules of each event/temporal relation. The complexity of frequent seasonal k-event pattern mining is $O(n^2 i^2 u^2) + O(|F_1| \cdot |F_{k-1}| \cdot r \cdot k^2 \cdot u)$.

STPM overall complexity: STPM complexity depends on the size of the search space ($O(n^h 3^{h^2})$), and the complexity of the mining process itself, i.e., $O(n \cdot |D_{SEQ}|) + O(n^2 i^2 u^2) + O(|F_1| \cdot |F_{k-1}| \cdot r \cdot k^2 \cdot u)$. While the parameters n, h, i, r and k depend on

the number of time series, others such as $|F_1|$, $|F_{k-1}|$ and u depend on the number of temporal sequences. Thus, given a time series dataset, STPM complexity is driven by two main factors: the number of time series and the number of temporal sequences.

5 APPROXIMATE STPM

5.1 Correlated Symbolic Time Series

Let X_S and Y_S be the symbolic series representing the time series X and Y , respectively, and Σ_X , Σ_Y be their symbolic alphabets.

Definition 5.1 (Entropy) The *entropy* of X_S , denoted as $H(X_S)$, is defined as

$$H(X_S) = - \sum_{x \in \Sigma_X} p(x) \cdot \log p(x) \quad (3)$$

where $p(x)$ is the probability of X_S . Intuitively, the entropy measures the uncertainty in the possible outcomes of X_S . The higher the $H(X_S)$, the more uncertain the outcome of X_S .

The conditional entropy $H(X_S|Y_S)$ quantifies the amount of information needed to describe the outcome of X_S , given the value of Y_S , and is defined as

$$H(X_S|Y_S) = - \sum_{x \in \Sigma_X} \sum_{y \in \Sigma_Y} p(x, y) \cdot \log \frac{p(x, y)}{p(y)} \quad (4)$$

where $p(x, y)$ is the joint probability of (X_S, Y_S) , and $p(y)$ is the probability of Y_S .

Definition 5.2 (Mutual information) The *mutual information* (MI) of two symbolic series X_S and Y_S , denoted as $I(X_S; Y_S)$, is defined as

$$I(X_S; Y_S) = \sum_{x \in \Sigma_X} \sum_{y \in \Sigma_Y} p(x, y) \cdot \log \frac{p(x, y)}{p(x) \cdot p(y)} \quad (5)$$

The MI represents the reduction of uncertainty of one variable (e.g., X_S), given the knowledge of another variable (e.g., Y_S). The larger $I(X_S; Y_S)$, the more information is shared between X_S and Y_S , and thus, the less uncertainty about one variable given the other.

Since $0 \leq I(X_S; Y_S) \leq \min(H(X_S), H(Y_S))$ [7], the MI value has no upper bound. To scale the MI into the range $[0 - 1]$, we use normalized mutual information as defined below.

Definition 5.3 (Normalized mutual information) The *normalized mutual information* (NMI) of two symbolic time series X_S and Y_S , denoted as $\tilde{I}(X_S; Y_S)$, is defined as

$$\tilde{I}(X_S; Y_S) = \frac{I(X_S; Y_S)}{H(X_S)} = 1 - \frac{H(X_S|Y_S)}{H(X_S)} \quad (6)$$

$\tilde{I}(X_S; Y_S)$ represents the reduction (in percentage) of the uncertainty of X_S due to knowing Y_S . Based on Eq. (6), a pair of variables (X_S, Y_S) has a mutual dependency if $\tilde{I}(X_S; Y_S) > 0$. Eq. (6) also shows that NMI is not symmetric, i.e., $\tilde{I}(X_S; Y_S) \neq \tilde{I}(Y_S; X_S)$.

Using Table 1, we have $I(C; D) = 0.39$. However, we do not know what the 0.39 reduction means in practice. Applying Eq. (6), we can compute NMI $\tilde{I}(C; D) = 0.41$, which says that the uncertainty of C is reduced by 41% given D . Moreover, we also have $\tilde{I}(D; C) = 0.40$, showing that $\tilde{I}(C; D) \neq \tilde{I}(D; C)$.

Definition 5.4 (Correlated symbolic time series) Let μ ($0 < \mu \leq 1$) be the mutual information threshold. We say that the two symbolic series X_S and Y_S are *correlated* iff $\tilde{I}(X_S; Y_S) \geq \mu \vee \tilde{I}(Y_S; X_S) \geq \mu$, and *uncorrelated* otherwise.

5.2 Lower Bound of the maxSeason

5.2.1 Derivation of the lower bound. Consider 2 symbolic series X_S and Y_S . Let X_1 be a temporal event in X_S , Y_1 be a temporal event in Y_S , and \mathcal{D}_{SYB} and \mathcal{D}_{SEQ} be the symbolic and the sequence

databases created from X_S and Y_S , respectively. We have the following relationship between $\tilde{I}(X_S; Y_S)$ in \mathcal{D}_{SYB} , and the maximum seasonal occurrence of (X_1, Y_1) in \mathcal{D}_{SEQ} as follows.

THEOREM 1. (Lower bound of the maximum seasonal occurrence) Let μ be the MI threshold. If the NMI $\tilde{I}(X_S; Y_S) \geq \mu$, then the maximum seasonal occurrence of (X_1, Y_1) in \mathcal{D}_{SEQ} has a lower bound:

$$\text{maxSeason}(X_1, Y_1) \geq \frac{\lambda_2 \cdot |\mathcal{D}_{SEQ}|}{\text{minDensity}} \cdot e^{W\left(\frac{\log \lambda_1^{1-\mu} \cdot \ln 2}{\lambda_2}\right)} \quad (7)$$

where: $\lambda_1 = \min\{p(X_i), \forall X_i \in X_S\}$ is the minimum probability of $X_i \in X_S$, and $\lambda_2 = p(Y_1)$ is the probability of $Y_1 \in Y_S$, and W is the Lambert function [6].

PROOF. The proof is provided in [12] due to the space limitations. \square

To compute the lower bound of $\text{maxSeason}(X_1, Y_1)$ in Eq. (7), several parameters need to be defined: λ_1 , λ_2 , and μ . Given \mathcal{D}_{SYB} , λ_1 and λ_2 can easily be determined since λ_1 is the minimum probability among all events $X_i \in X_S$, and λ_2 is the probability of $Y_1 \in Y_S$. How to determine the value of μ is discussed in Section 5.3.

Interpretation of the lower bound of the maximum seasonal occurrence: Theorem 1 says that, given an MI threshold μ , if the two symbolic series X_S and Y_S are correlated, i.e., $\tilde{I}(X_S; Y_S) \geq \mu$, then the maximum seasonal occurrence of an event pair in (X_S, Y_S) is at least the lower bound in Eq. (7). Combining Theorem 1 and Lemma 3, we can conclude that given a pair of symbolic series (X_S, Y_S) , if its event pair (X_1, Y_1) has a maximum seasonal occurrence less than the lower bound in Eq. (7), then any 2-event pattern P formed by that event pair also has a maximum seasonal occurrence less than that lower bound. This allows us to construct the approximate STPM algorithm, discussed in the next section.

5.3 Using the Bound to Approximate STPM

5.3.1 Correlation graph. Using Theorem 1, we propose to approximate STPM by performing STPM mining only on the set of correlated symbolic series $\mathcal{X}_C \subseteq \mathcal{X}$. We first define the correlation graph.

Definition 5.5 (Correlation graph) A *correlation graph* is an *undirected graph* $G_C = (V, E)$ where V is the set of vertices, and E is the set of edges. Each vertex $v \in V$ represents one symbolic series $X_S \in \mathcal{X}_C$. There is an edge e_{uv} between a vertex u containing X_S , and a vertex v containing Y_S iff $\tilde{I}(X_S; Y_S) \geq \mu \vee \tilde{I}(Y_S; X_S) \geq \mu$.

Fig. 8 shows an example of the correlation graph G_C built from \mathcal{D}_{SYB} in Table 1. Here, each node corresponds to one time series. There is an edge between two nodes if their NMI is at least μ . The weight on each edge is the NMI between two nodes.

Constructing the correlation graph: Given a symbolic database \mathcal{D}_{SYB} , the correlation graph G_C can easily be constructed by computing the NMI for each symbolic series pair, and comparing it against the threshold μ . A symbolic series pair is included in G_C iff their NMI is at least μ .

Algorithm 2: Approximate STPM using MI

Input: A set of time series \mathcal{X} , the thresholds: $maxPeriod$, $minDensity$, $disInterval$, $minSeason$

Output: The set of frequent seasonal temporal patterns \mathcal{P}

- 1: convert \mathcal{X} to \mathcal{D}_{SYB} and \mathcal{D}_{SEQ} ;
- 2: scan \mathcal{D}_{SYB} to compute the probability of each event and event pair;
- 3: **foreach** pair of symbolic time series $(X_S, Y_S) \in \mathcal{D}_{SYB}$ **do**
- 4: Compute $\tilde{I}(X_S; Y_S)$ and $\tilde{I}(Y_S; X_S)$;
- 5: Compute μ ;
- 6: **if** $\tilde{I}(X_S; Y_S) \geq \mu \vee \tilde{I}(Y_S; X_S) \geq \mu$ **then**
- 7: Insert X_S and Y_S into \mathcal{X}_C ;
- 8: Create an edge between X_S and Y_S in G_C ;
- 9: **foreach** $X_S \in \mathcal{X}_C$ **do**
- 10: Mine frequent seasonal single events from X_S ;
- 11: EventPairs \leftarrow Cartesian(F_1, F_1);
- 12: **foreach** event pair (E_i, E_j) in EventPairs **do**
- 13: **if** there is an edge between X_S and Y_S in G_C **then**
- 14: Mine frequent seasonal patterns for (E_i, E_j) ;
- 15: **if** $k \geq 3$ **then**
- 16: Perform STPM using HLH_1 and HLH_{k-1} ;

Setting the value of μ : While NMI can easily be computed using Eq. (6), it is not trivial how to set the value of μ . Here, we use the lower bound of the $maxSeason$ in Eq. (7) to determine μ .

COROLLARY 1.1. *The maximum seasonal occurrence of an event pair $(X_1, Y_1) \in (X_S, Y_S)$ in \mathcal{D}_{SEQ} is at least $minSeason$ if $\tilde{I}(X_S; Y_S)$ is at least μ , where:*

$$\mu \geq \begin{cases} 1 - \frac{\lambda_2}{e \cdot \ln 2 \cdot \log \frac{1}{\lambda_1}}, & \text{if } 0 \leq \rho \leq \frac{1}{e} \\ 1 - \frac{\rho \cdot \lambda_2 \cdot \log \rho}{\ln 2 \cdot \log \lambda_1}, & \text{otherwise} \end{cases}, \text{ with: } \rho = \frac{minSeason \cdot minDensity}{\lambda_2 \cdot |\mathcal{D}_{SEQ}|} \quad (8)$$

Note that μ in Eq. (8) only ensures that the $maxSeason$ of the event pair (X_1, Y_1) is at least $minSeason$. Thus, given (X_S, Y_S) , μ has to be computed for each event pair in (X_S, Y_S) . The final chosen μ value to be compared against $\tilde{I}(X_S; Y_S)$ is the minimum μ value among all the event pairs in (X_S, Y_S) .

5.3.2 Approximate STPM using the correlation graph. Using the correlation graph G_C , the approximate STPM is described in Algorithm 2. First, \mathcal{D}_{SYB} is scanned once to compute the probability of each single event and pair of events (line 2). Next, NMI and μ are computed for each pair of symbolic series (X_S, Y_S) in \mathcal{D}_{SYB} (lines 4-5). Then, only pairs whose $\tilde{I}(X_S; Y_S)$ or $\tilde{I}(Y_S; X_S)$ is at least μ are inserted into \mathcal{X}_C , and an edge between X_S and Y_S is created (lines 6-8). Next, only the correlated symbolic series in \mathcal{X}_C are used to mine frequent seasonal single events (lines 9-10). For mining frequent seasonal 2-event patterns, G_C is used to filter candidate 2-event groups: for each event pair (E_i, E_j) , we check whether there is an edge between their corresponding symbolic series in G_C . If so, we proceed by verifying the maximum seasonal occurrence of (E_i, E_j) and determining the frequent seasonal patterns of (E_i, E_j) as in the exact STPM (lines 12-14). Otherwise, (E_i, E_j) is eliminated from the mining of HLH_2 . For mining frequent seasonal k -event ($k \geq 3$) patterns onwards, the exact STPM is used (lines 15-16).

5.3.3 Complexity analysis. To compute NMI and μ , we only have to scan \mathcal{D}_{SYB} once to calculate the probability for each single event and pair of events. Thus, the cost of NMI and μ computations is $|\mathcal{D}_{SYB}|$. On the other hand, the complexities of the exact STPM for HLH_1 and HLH_2 are $O(n \cdot |\mathcal{D}_{SEQ}|) + O(n^2 i^2 u^2)$ (Sections 4.3 and 4.4). Thus, the approximate STPM is significantly faster than STPM.

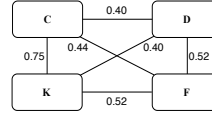


Figure 8: Corr. graph

Datasets	#seq.	#time series	#events	#ins./seq.
RE (real)	1,460	21	102	93
SC (real)	1,249	14	56	55
INF (real)	608	25	124	48
HFM (real)	730	24	115	40
RE (syn.)	$1,460 \times 10^3$	10^4	48,500	38,012
SC (syn.)	$1,249 \times 10^3$	10^4	40,020	37,106
INF (syn.)	608×10^4	10^4	49,600	40,623
HFM (syn.)	730×10^4	10^4	47,825	41,241

Table 4: Datasets Summary

6 EXPERIMENTAL EVALUATION

We evaluate STPM (exact and approximate), using real-world datasets from three application domains: renewable energy, smart city, and health (influenza, and hand-foot-mouth diseases). The evaluation is both qualitative (to assess the quality of extracted patterns) and quantitative (to evaluate the scalability and efficiency of STPM). Due to space limitations, we only present here the most important results, and discuss other findings in the technical report [12].

6.1 Experimental Setup

Datasets: For the *renewable energy* (RE) domain, we use the renewable energy data [27] and weather data [31] from Spain. For the *smart city* (SC), we use the traffic and weather dataset [24] from New York City. For the health domain, we use the *influenza* (INF) and *hand-foot-mouth* (HFM) datasets [5] and weather data [31] from Kawasaki, Japan. Besides real-world datasets, we also generate synthetic datasets used in the scalability evaluation. Specifically, starting from the real-world datasets, we generate 1000 times more sequences and 10000 synthetic time series for each of them. Table 4 summarizes the characteristics of real-world and synthetic datasets.

Baseline method: Our exact method is referred to as E-STPM, and the approximate one as A-STPM. Since our work is the first that studies frequent seasonal temporal pattern mining, there does not exist an exact baseline to compare against STPM. However, we adapt the state-of-the-art method for recurring itemset pattern mining PS-growth [14] to find seasonal temporal patterns. Specifically, the adaptation is done through 2-phase process: (1) PS-growth is applied to find frequent recurring temporal events, and (2), mine temporal patterns from extracted events. The adapted PS-growth is referred to as APS-growth.

Infrastructure: The experiments are run on a virtual machine with 32 AMD EPYC cores (2GHz), 512 GB RAM, and 1 TB storage.

Parameters: Table 5 lists the parameters and their values used in our experiments. The two measures $maxPeriod$ and $minDensity$ are expressed in percentage of \mathcal{D}_{SEQ} .

6.2 Qualitative Evaluation

Our goal is to gain insights from the extracted seasonal temporal patterns. Table 7 lists some interesting seasonal patterns found in the datasets. Patterns P1-P3 are extracted from RE, showing that high renewable energy generation and high electricity demand occur seasonally and often at specific *season* throughout the year. Patterns P4-P7 are extracted from INF and HFM, showing the detection of seasonal diseases. Finally, how weather affects traffic is shown in patterns P8-P11 extracted from SC.

6.3 Quantitative Evaluation

6.3.1 Baseline comparison on real-world datasets. We compare E-STPM and A-STPM with the baseline in terms of the runtime and memory usage. Figs. 9, 10, 11 and 12 show the comparison on RE and INF datasets. The experimental results on the other datasets are reported in the full paper [12].

As shown in Figs. 9 and 10, A-STPM achieves the best runtime among all methods, and E-STPM has better runtime than the baseline. On the tested datasets, the range and average speedups of A-STPM compared to other methods are: [1.5-4.7] and 2.6 (E-STPM),

Table 5: Parameters and values

Params	Values (User-defined)
<i>maxPeriod</i>	0.2%, 0.4%, 0.6%, 0.8%, 1.0%
<i>minDensity</i>	0.5%, 0.75%, 1.0%, 1.25%, 1.5%
<i>minSeason</i>	4, 8, 12, 16, 20
<i>distInterval</i>	[90, 270] (RE, SC), [30, 90] (INF, HFM)

Table 6: A-STPM Accuracy

# minSeason	minDensity (%)					
	RE (real)			INF (real)		
	0.5	0.75	1	0.5	0.75	1
8	81	82	86	81	83	87
12	84	86	92	88	90	93
16	94	95	100	95	96	100
20	97	100	100	100	100	100

Table 8: Pruned Time Series and Events from A-STPM

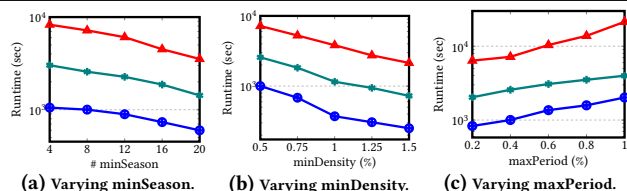
# Attr.	RE						INF					
	Pruned Time Series (%)			Pruned Events (%)			Pruned Time Series (%)			Pruned Events (%)		
	12-0.5%	16-0.75%	20-1.0%	12-0.5%	16-0.75%	20-1.0%	12-0.5%	16-0.75%	20-1.0%	12-0.5%	16-0.75%	20-1.0%
2000	35.20	32.10	26.80	27.22	23.53	19.03	42.60	36.75	29.70	28.63	26.12	22.10
4000	33.05	29.15	22.05	25.24	22.41	17.95	35.70	31.03	24.80	27.35	25.77	22.01
6000	30.25	26.32	19.55	24.75	21.60	17.28	33.22	28.78	22.13	26.98	25.29	20.81
8000	29.48	25.38	19.15	24.70	21.12	16.96	31.75	28.51	21.58	26.74	24.52	20.74
10000	28.59	24.87	18.91	24.50	21.07	16.69	31.06	26.48	21.15	26.61	24.36	20.27

Table 7: Summary of Interesting Seasonal Patterns

Patterns	minDensity (%)	maxPeriod (%)	# minSeason	Seasonal occurrence
(P1) Strong Wind \geq High Wind Power Generation	0.5	0.4	12	December, January, February
(P2) Low Temperature \geq High Energy Consumption	0.5	0.4	12	December, January, February
(P3) Very Few Cloud \geq Very High Temperature \cap High Solar Power Generation	0.75	0.6	8	July, August
(P4) High Humidity \geq Very Low Temperature \rightarrow Very High Influenza Cases	0.5	0.4	12	January, February
(P5) Strong Wind \geq Heavy Rain \geq High Influenza Cases	0.5	0.4	12	January, February
(P6) Low Humidity \geq High Temperature \geq Very High Hand-Foot-Mouth Disease Cases	1.0	0.6	12	May, June
(P7) Very High Temperature \geq High Wind \geq High Hand-Foot-Mouth Disease Cases	1.0	0.6	12	May, June
(P8) High Temperature \geq Strong Wind \rightarrow High Congestion	0.5	0.6	8	July, August
(P9) Strong Wind \geq Unclear Visibility \geq High Congestion	0.5	0.6	8	July, August
(P10) Heavy Rain \geq Unclear Visibility \geq High Lane-Blocked	0.4	0.8	8	July, August
(P11) Heavy Rain \geq Strong Wind \geq High Flow-Incident	0.4	0.8	8	July, August

Table 9: The Accuracy of A-STPM on Syn. Data

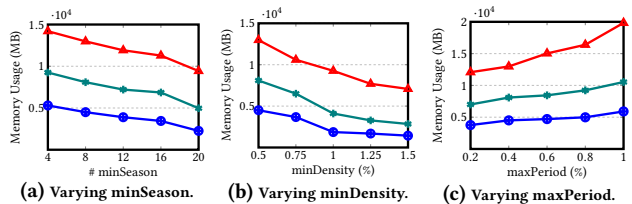
# Attr.	RE			INF		
	Accuracy (%)			Accuracy (%)		
	12-0.5%	16-0.75%	20-1.0%	12-0.5%	16-0.75%	20-1.0%
2000	85	96	100	89	96	100
4000	86	96	100	90	98	100
6000	86	96	100	91	98	100
8000	88	97	100	93	98	100
10000	89	98	100	93	98	100



(a) Varying minSeason. (b) Varying minDensity. (c) Varying maxPeriod.



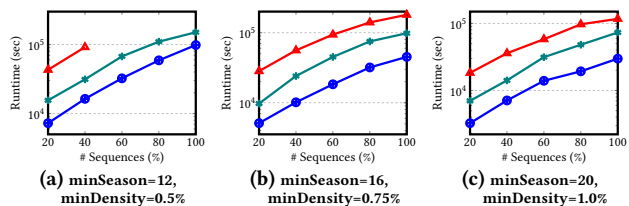
Figure 9: Runtime Comparison on RE (real-world)



(a) Varying minSeason. (b) Varying minDensity. (c) Varying maxPeriod.



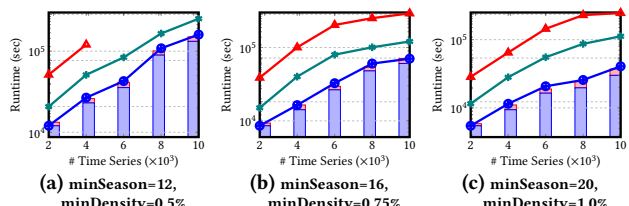
Figure 11: Memory Usage Comparison on RE (real-world)



(a) minSeason=12, minDensity=0.5% (b) minSeason=16, minDensity=0.75% (c) minSeason=20, minDensity=1.0%



Figure 13: Scalability: Varying #Sequences on RE (synthetic)



(a) minSeason=12, minDensity=0.5% (b) minSeason=16, minDensity=0.75% (c) minSeason=20, minDensity=1.0%

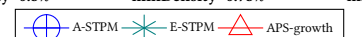
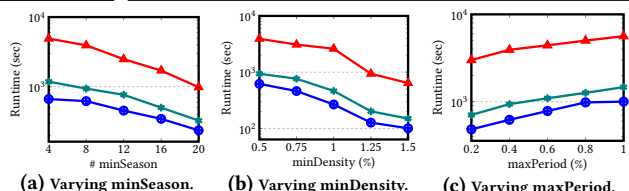


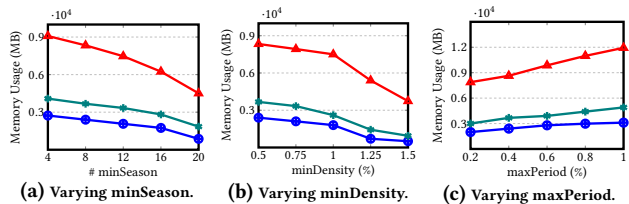
Figure 15: Scalability: Varying #TimeSeries on RE (synthetic)



(a) Varying minSeason. (b) Varying minDensity. (c) Varying maxPeriod.



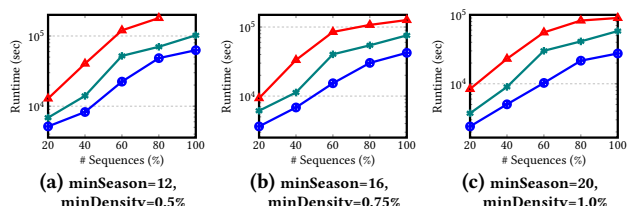
Figure 10: Runtime Comparison on INF (real-world)



(a) Varying minSeason. (b) Varying minDensity. (c) Varying maxPeriod.



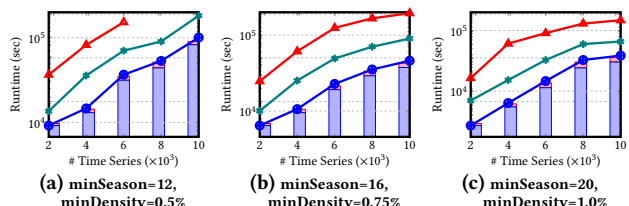
Figure 12: Memory Usage Comparison on INF (real-world)



(a) minSeason=12, minDensity=0.5% (b) minSeason=16, minDensity=0.75% (c) minSeason=20, minDensity=1.0%



Figure 14: Scalability: Varying #Sequences on INF (synthetic)



(a) minSeason=12, minDensity=0.5% (b) minSeason=16, minDensity=0.75% (c) minSeason=20, minDensity=1.0%



Figure 16: Scalability: Varying #TimeSeries on INF (synthetic)

and [5.2-10.6] and 7.1 (APS-growth). The speedup of E-STPM compared to the baseline is [3.5-7.2] and 4.3 on average. Note that

the times to compute MI and μ for RE and INF in Figs. 9 and 10 are only 2.6 and 1.4 seconds, respectively. Moreover, A-STPM is

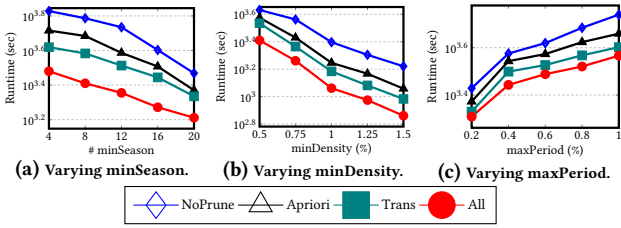


Figure 17: Pruning Techniques of E-STPM on RE (real-world)

most efficient, i.e., achieves highest speedup and memory saving, when the *minSeason* threshold is low, e.g., *minSeason* = 4. This is because there are typically many patterns with few seasonal occurrences. Thus, using A-STPM to prune uncorrelated time series early helps save computational time and resources. However, the speedup comes at the cost of a small loss in accuracy (discussed in Section 6.3.4).

In terms of memory consumption, as shown in Figs. 11 and 12, A-STPM is the most efficient method, while E-STPM is more efficient than the baseline. The range and the average memory consumption of A-STPM compared to other methods are: [1.4-2.7] and 1.8 (E-STPM), and [2.7-7.6] and 3.9 (APS-growth). The memory usage of E-STPM compared to the baseline is [1.5-4.1] and 2.3 on average.

6.3.2 Scalability evaluation on synthetic datasets. As discussed in Section 4, the complexity of STPM is driven by two main factors: (1) the number of temporal sequences, and (2) the number of time series. The evaluation on real-world datasets has shown that E-STPM and A-STPM outperform the baseline significantly in both runtimes and memory usage. However, to further evaluate STPM scalability, we scale these two factors on synthetic datasets (reported in Table 4). We evaluate the scalability using two configurations: varying the number of sequences, and varying the number of time series.

Figs. 13 and 14 show the runtimes of A-STPM, E-STPM and the baseline when the number of sequences changes (y-axis is in log scale). We obtain the range and average speedups of A-STPM are: [1.6-3.2] and 2.2 (E-STPM), and [3.1-6.4] and 4.6 (APS-growth). Similarly, the range and average speedup of E-STPM compared to APS-growth is [1.9-4.3] and 3.2. We note that the baseline fails for larger configurations because of memory in this scalability study, i.e., on the synthetic RE at 60% sequences ($\approx 8 \times 10^5$) (Fig. 13a) and on the synthetic INF at 100% sequences ($\approx 6 \times 10^5$) (Fig. 14a), showing that A-STPM and E-STPM can scale well on big datasets while the baseline cannot.

Figs. 15 and 16 compare the runtimes of A-STPM, E-STPM and APS-growth when changing the number of time series. We obtain the range and average speedups of A-STPM are: [1.7-3.5] and 2.3 (E-STPM), and [3.8-9.5] and 5.3 (APS-growth), and of E-STPM is [2.3-4.4] and 3.2 (APS-growth). The baseline also fails at large configurations in this study, i.e., when # Time Series ≥ 6000 on the synthetic RE (Fig. 15a), and ≥ 8000 on the synthetic INF (Fig. 16a).

Furthermore, we provide the computation time of MI and μ in Figs. 15 and 16 by adding an additional bar chart for A-STPM. Each bar represents the runtime of A-STPM with two separate components: the time to compute MI and μ (top red), and the mining time (bottom blue). We note that for each dataset, we only need to compute MI once (the computed MIs are used across different *minSeason* and *minDensity* thresholds), while the computation of μ is negligible (in milliseconds using Eq. (8)). Thus, the MI and μ computation times, for example, in Figs. 15a, 15b, and 15c, are added only for comparison and are not all actually used.

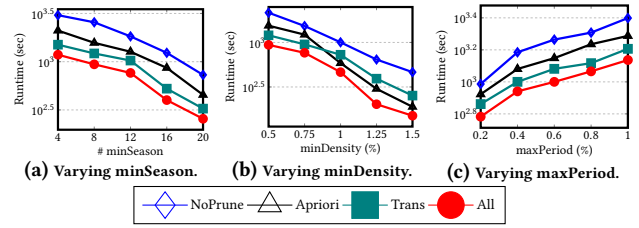


Figure 18: Pruning Techniques of E-STPM on INF (real-world)

Finally, we provide the percentage of time series and events pruned by A-STPM in the scalability test in Table 8. Here, we can see that low *minSeason* and *minDensity* lead to more time series (events) to be pruned. This is because *minSeason* and *minDensity* have an inverse relationship with μ , therefore, low *minSeason* and *minDensity* result in higher μ , and thus, more pruned time series.

6.3.3 Evaluation of the pruning techniques in E-STPM. To understand how effective the proposed pruning techniques are, we compare different versions of E-STPM: (1) NoPrune: E-STPM with no pruning, (2) Apriori: E-STPM with Apriori-like pruning (Lemmas 1, 2, 3), (3) Trans: E-STPM with transitivity-based pruning (Lemmas 4, 5), and (4) All: E-STPM applied both pruning techniques.

We use three different configurations that vary: the minimum season, the minimum density, and the maximum period. Figs. 17, 18 show the results (the y-axis is in log scale). It can be seen that (All)-E-STPM achieves the best performance among all versions. Its speedup w.r.t. (NoPrune)-E-STPM ranges from 3 up to 6 depending on the configurations, showing that the proposed prunings are very effective in improving E-STPM performance. Furthermore, (Trans)-E-STPM delivers larger speedup than (Apriori)-E-STPM. The average speedup is from 2 to 5 for (Trans)-E-STPM, and from 1.5 to 4 for (Apriori)-E-STPM. However, applying both always yields better speedup than applying either of them.

6.3.4 Evaluation of A-STPM. We proceed to evaluate the accuracy of A-STPM by comparing the patterns extracted by A-STPM and E-STPM. Table 6 shows the accuracies of A-STPM for different *minSeason* and *minDensity* on the real-world datasets. It is seen that, A-STPM obtains high accuracy ($\geq 81\%$) when *minSeason* and *minDensity* are low, e.g., *minSeason* = 8 and *minDensity* = 0.5%, and very high accuracy ($\geq 95\%$) when *minSeason* and *minDensity* are high, e.g., *minSeason* = 16 and *minDensity* = 0.75%. Similarly, Table 9 shows the accuracies of A-STPM on the synthetic datasets: very high accuracy ($\geq 96\%$) when *minSeason* and *minDensity* are high, e.g., *minSeason* = 16 and *minDensity* = 0.75%.

7 CONCLUSION AND FUTURE WORK

This paper presents our efficient Frequent Seasonal Temporal Pattern Mining from Time Series (FreqSTPFTS) approach that offers: (1) the first solution for Seasonal Temporal Pattern Mining (STPM), (2) the efficient and exact Seasonal Temporal Pattern Mining (E-STPM) algorithm that employs the efficient data structures and pruning techniques to achieve fast mining, and (3) the approximate A-STPM that uses mutual information to prune unpromising time series and allows STPM to scale on big datasets. Extensive experiments conducted on real-world and synthetic datasets show that both A-STPM and E-STPM outperform the baseline, consume less memory, and scale well to big datasets. Compared to the baseline, the approximate A-STPM delivers up to an order of magnitude speedup. In future work, we plan to extend STPM to prune at the event level to further improve its performance.

REFERENCES

- [1] James F Allen. 1983. Maintaining knowledge about temporal intervals. *Commun. ACM* 26 (1983).
- [2] Komate Amphawan, Philippe Lenca, and Athasit Surarerks. 2009. Mining top-k periodic-frequent pattern from transactional databases without support threshold. In *International conference on advances in information technology*. Springer, 18–29.
- [3] P Cameron, JG Hocking, and SA Naimpally. 1974. Nearness—a better approach to continuity and limits. *The American Mathematical Monthly* 81, 7 (1974), 739–745.
- [4] Y. Chen, W. Peng, and S. Lee. 2015. Mining Temporal Patterns in Time Interval-Based Data. *TKDE* 27 (2015).
- [5] Kawasaki city infectious disease surveillance system. 2021. KIDSS. <https://kidss.city.kawasaki.jp/>
- [6] Robert M Corless, Gaston H Gonnet, David EG Hare, David J Jeffrey, and Donald E Knuth. 1996. On the LambertW function. *Advances in Computational mathematics* 5, 1 (1996), 329–359.
- [7] Thomas M Cover and Joy A Thomas. 2012. *Elements of information theory*. John Wiley & Sons.
- [8] Philippe Fournier-Viger, Ying Wang, Peng Yang, Jerry Chun-Wei Lin, Unil Yun, and Rage Uday Kiran. 2022. Tspin: Mining top-k stable periodic patterns. *Applied Intelligence* 52, 6 (2022), 6917–6938.
- [9] Jiawei Han, Guozhu Dong, and Yiwen Yin. 1999. Efficient mining of partial periodic patterns in time series database. In *Proceedings 15th International Conference on Data Engineering (Cat. No. 99CB36337)*. IEEE, 106–115.
- [10] Jiawei Han, Wan Gong, and Yiwen Yin. 1998. Mining Segment-Wise Periodic Patterns in Time-Related Databases.. In *KDD*, Vol. 98. 214–218.
- [11] Van Long Ho, Nguyen Ho, and Torben Bach Pedersen. 2022. Efficient Temporal Pattern Mining in Big Time Series Using Mutual Information. In *PVLDB*, Vol. 15.
- [12] Van Long Ho, Nguyen Ho, and Torben Bach Pedersen. 2022. Mining Seasonal Temporal Patterns in Big Time Series. *arXiv preprint arXiv:2206.14604* (2022). <https://arxiv.org/abs/2206.14604>
- [13] Jen-Wei Huang, Chi-Yao Tseng, Jian-Chih Ou, and Ming-Syan Chen. 2008. A general model for sequential pattern mining with a progressive database. *IEEE Transactions on knowledge and data engineering* 20, 9 (2008), 1153–1167.
- [14] Rage Uday Kiran, Alampally Anirudh, Chennupati Saideep, Masashi Toyoda, P Krishna Reddy, and Masaru Kitsuregawa. 2019. Finding periodic-frequent patterns in temporal databases using periodic summaries. *Data Science and Pattern Recognition* 3, 2 (2019), 24–46.
- [15] R Uday Kiran, Masaru Kitsuregawa, and P Krishna Reddy. 2016. Efficient discovery of periodic-frequent patterns in very large databases. *Journal of Systems and Software* 112 (2016), 110–121.
- [16] R Uday Kiran, C Saideep, Koji Zettsu, Masashi Toyoda, Masaru Kitsuregawa, and P Krishna Reddy. 2019. Discovering partial periodic spatial patterns in spatiotemporal databases. In *2019 IEEE International Conference on Big Data (Big Data)*. IEEE, 233–238.
- [17] R Uday Kiran, Haichuan Shang, Masashi Toyoda, and Masaru Kitsuregawa. 2015. Discovering Recurring Patterns in Time Series. In *EDBT*. 97–108.
- [18] R Uday Kiran, Yutaka Watanobe, Bhaskar Chaudhury, Koji Zettsu, Masashi Toyoda, and Masaru Kitsuregawa. 2020. Discovering maximal periodic-frequent patterns in very large temporal databases. In *2020 IEEE 7th International Conference on Data Science and Advanced Analytics (DSAA)*. IEEE, 11–20.
- [19] Hoang Thanh Lam, Fabian Mörchen, Dmitriy Fradkin, and Toon Calders. 2014. Mining compressing sequential patterns. *Statistical Analysis and Data Mining: The ASA Data Science Journal* 7, 1 (2014), 34–52.
- [20] Zed Lee, Tony Lindgren, and Panagiotis Papapetrou. 2020. Z-miner: an efficient method for mining frequent arrangements of event intervals. In *Proceedings of the 26th ACM SIGKDD International Conference on Knowledge Discovery & Data Mining*. 524–534.
- [21] Jessica Lin, Eamonn Keogh, Stefano Lonardi, and Bill Chiu. 2003. A symbolic representation of time series, with implications for streaming algorithms. In *Proceedings of the 8th ACM SIGMOD workshop on Research issues in data mining and knowledge discovery*. 2–11.
- [22] Honglei Liu, Fangqiu Han, Hongjun Zhou, Xifeng Yan, and Kenneth S Kosik. 2016. Fast motif discovery in short sequences. In *2016 IEEE 32nd International Conference on Data Engineering (ICDE)*. IEEE, 1158–1169.
- [23] Yasser Mohammad and Toyoaki Nishida. 2013. Approximately recurring motif discovery using shift density estimation. In *International Conference on Industrial, Engineering and Other Applications of Applied Intelligent Systems*. Springer, 141–150.
- [24] Sobhan Moosavi, Mohammad Hossein Samavatian, Arnab Nandi, Srinivasan Parthasarathy, and Rajiv Ramnath. 2019. Short and long-term pattern discovery over large-scale geo-spatiotemporal data. In *Proceedings of the 25th ACM SIGKDD International Conference on Knowledge Discovery & Data Mining*. 2905–2913.
- [25] Panagiotis Papapetrou, George Kollios, Stan Sclaroff, and Dimitrios Gunopoulos. 2009. Mining frequent arrangements of temporal intervals. *KAIS* 21 (2009).
- [26] Dhaval Patel, Wynne Hsu, and Mong Li Lee. 2008. Mining relationships among interval-based events for classification. In *SIGMOD*.
- [27] ENTSO-E Transparency Platform. 2019. ENTSO-E. <https://transparency.entsoe.eu/dashboard/show>
- [28] Amit Kumar Sharma and Dhaval Patel. 2018. Stipa: A memory efficient technique for interval pattern discovery. In *2018 IEEE International Conference on Big Data (Big Data)*. IEEE, 1767–1776.
- [29] Syed Khairuzzaman Tanbeer, Chowdhury Farhan Ahmed, Byeong-Soo Jeong, and Young-Koo Lee. 2009. Discovering periodic-frequent patterns in transactional databases. In *Pacific-Asia Conference on Knowledge Discovery and Data Mining*. Springer, 242–253.
- [30] R Uday Kiran and P Krishna Reddy. 2010. Towards efficient mining of periodic-frequent patterns in transactional databases. In *International Conference on Database and Expert Systems Applications*. Springer, 194–208.
- [31] Open Weather. 2021. Open Weather. <https://openweathermap.org/>
- [32] Mingming Zhang, Peng Wang, and Wei Wang. 2022. Efficient Consensus Motif Discovery of All Lengths in Multiple Time Series. In *International Conference on Database Systems for Advanced Applications*. Springer, 540–555.

A DETAILED PROOFS OF COMPLEXITIES, LEMMAS AND THEOREMS

A.1 Mutual exclusive property of temporal relations

Property 1. (Mutual exclusive) Consider the set of temporal relations $\mathfrak{R} = \{\text{Follows}, \text{Contains}, \text{Overlaps}\}$. Let E_i and E_j be two temporal events, and e_i occurring during $[t_{s_i}, t_{e_i}]$, e_j occurring during $[t_{s_j}, t_{e_j}]$ be their corresponding event instances, and ϵ be the tolerance buffer. The relations in \mathfrak{R} are mutually exclusive on E_i and E_j .

PROOF. * **Case 1:** Assume the relation **Follows**($E_{i \triangleright e_i}, E_{j \triangleright e_j}$) holds between E_i and E_j . Thus, we have:

$$t_{e_i} \pm \epsilon \leq t_{s_j} \quad (9)$$

and:

$$t_{s_j} < t_{e_j} \Rightarrow t_{e_i} \pm \epsilon < t_{e_j} \quad (10)$$

Hence, **Contains**($E_{i \triangleright e_i}, E_{j \triangleright e_j}$) cannot exist between E_i and E_j , since **Contains**($E_{i \triangleright e_i}, E_{j \triangleright e_j}$) holds iff $(t_{s_i} \leq t_{s_j}) \wedge (t_{e_i} \pm \epsilon \geq t_{e_j})$ (contradict Eq. (10)). Similarly, **Overlaps**($E_{i \triangleright e_i}, E_{j \triangleright e_j}$) cannot exist between E_i and E_j since **Overlaps**($E_{i \triangleright e_i}, E_{j \triangleright e_j}$) holds iff $(t_{s_i} < t_{s_j}) \wedge (t_{e_i} \pm \epsilon < t_{e_j}) \wedge (t_{e_i} - t_{s_j} \geq d_0 \pm \epsilon)$ (contradict Eq. (9)).

In conclusion, if **Follows**($E_{i \triangleright e_i}, E_{j \triangleright e_j}$) holds between E_i and E_j , then the two remaining relations cannot exist between E_i and E_j .

* **Case 2:** Assume the relation **Contains**($E_{i \triangleright e_i}, E_{j \triangleright e_j}$) holds between E_i and E_j . Thus, we have:

$$t_{s_i} \leq t_{s_j} \quad (11)$$

$$t_{e_i} \pm \epsilon \geq t_{e_j} \quad (12)$$

Hence, **Follows**($E_{i \triangleright e_i}, E_{j \triangleright e_j}$) cannot exist between E_i and E_j since **Follows**($E_{i \triangleright e_i}, E_{j \triangleright e_j}$) holds iff $t_{e_i} \pm \epsilon < t_{e_j}$ (contradict Eq. (12)).

Similarly, **Overlaps**($E_{i \triangleright e_i}, E_{j \triangleright e_j}$) cannot exist between E_i and E_j , since **Overlaps**($E_{i \triangleright e_i}, E_{j \triangleright e_j}$) holds iff $(t_{s_i} < t_{s_j}) \wedge (t_{e_i} \pm \epsilon < t_{e_j}) \wedge (t_{e_i} - t_{s_j} \geq d_0 \pm \epsilon)$ (contradict Eq. (12)).

In conclusion, if **Contains**($E_{i \triangleright e_i}, E_{j \triangleright e_j}$) holds between E_i and E_j , then the two remaining relations cannot exist between E_i and E_j .

* **Case 3:** Assume the relation **Overlaps**($E_{i \triangleright e_i}, E_{j \triangleright e_j}$) holds between E_i and E_j . Thus, we have:

$$t_{s_i} < t_{s_j} \quad (13)$$

$$t_{e_i} \pm \epsilon < t_{e_j} \quad (14)$$

$$t_{e_i} - t_{s_j} \geq d_0 \pm \epsilon \Rightarrow t_{s_j} \leq t_{e_i} - d_0 \pm \epsilon \quad (15)$$

Hence, **Follows**($E_{i \triangleright e_i}, E_{j \triangleright e_j}$) cannot exist between E_i and E_j , since **Follows**($E_{i \triangleright e_i}, E_{j \triangleright e_j}$) holds iff $t_{e_i} \pm \epsilon < t_{s_j}$ (contradict Eq. (15)).

Similarly, **Contains**($E_{i \triangleright e_i}, E_{j \triangleright e_j}$) cannot exist between E_i and E_j , since **Contains**($E_{i \triangleright e_i}, E_{j \triangleright e_j}$) holds iff $t_{e_i} \pm \epsilon \geq t_{e_j}$ (contradict Eq. (14)).

In conclusion, if **Overlaps**($E_{i \triangleright e_i}, E_{j \triangleright e_j}$) holds between E_i and E_j , then the two remaining relations cannot exist between E_i and E_j . \square

A.2 Lemma 1

Lemma 1. Let G_E be a group of temporal events, and G'_E be a subset of G_E , i.e., $G'_E \subseteq G_E$. Then $\text{maxSeason}(G'_E) \geq \text{maxSeason}(G_E)$.

PROOF.

$$\text{maxSeason}(G'_E) = \frac{|SUP^{G'_E}|}{\text{minDensity}}$$

$$\text{maxSeason}(G_E) = \frac{|SUP^{G_E}|}{\text{minDensity}}$$

Since : $|SUP^{G'_E}| \geq |SUP^{G_E}|$ (Derived directly from Def. 3.15)
 $\Rightarrow \text{maxSeason}(G'_E) \geq \text{maxSeason}(G_E)$ \square

A.3 Lemma 2

Lemma 2. Let P be a temporal pattern, and P' be a sub-pattern of P , i.e., $P' \subseteq P$. Then $\text{maxSeason}(P') \geq \text{maxSeason}(P)$.

PROOF.

$$\text{maxSeason}(P') = \frac{|SUP^{P'}|}{\text{minDensity}}$$

$$\text{maxSeason}(P) = \frac{|SUP^P|}{\text{minDensity}}$$

Since : $|SUP^{P'}| \geq |SUP^P|$ (Derived directly from Def. 3.15)
 $\Rightarrow \text{maxSeason}(P') \geq \text{maxSeason}(P)$ \square

A.4 Mining frequent seasonal single event

Complexity: The complexity of finding frequent seasonal single events is $O(n \cdot |\mathcal{D}_{\text{SEQ}}|)$, where n is the number of distinct events.

PROOF. Computing maxSeason for each event E_i takes $O(|\mathcal{D}_{\text{SEQ}}|)$. Thus, computing maxSeason for n events takes $O(n \cdot |\mathcal{D}_{\text{SEQ}}|)$. Moreover, for each candidate event E_i , identifying the set of seasons \mathcal{PS} takes $O(|SUP^{E_i}|)$. We have potentially n events. And thus, it takes $O(n \cdot |SUP^{E_i}|)$. The overall complexity is: $O(n \cdot |\mathcal{D}_{\text{SEQ}}| + n \cdot |SUP^{E_i}|) \sim O(n \cdot |\mathcal{D}_{\text{SEQ}}|)$. \square

A.5 Lemma 3

Lemma 3. Let P be a k -event temporal pattern formed by an k -event group (E_1, \dots, E_k) . Then, $\text{maxSeason}(P) \leq \text{maxSeason}(E_1, \dots, E_k)$.

PROOF. Derived directly from Def. 3.15, Eqs. (1) and (2). \square

A.6 Search space of STPM

Complexity: The search space of finding seasonal temporal patterns is $O(n^h 3^{h^2})$, where n is the number of distinct events in \mathcal{D}_{SEQ} , and h is the maximal length of a temporal pattern.

PROOF. The number of seasonal single events is: $N_1 = n \sim O(n)$. For mining 2-event groups, the number of permutations of n distinct events taken 2 at a time is: $P(n, 2)$. However, since the same event can form a pair of events with itself, the total number of 2-event groups is: $N_2 = P(n, 2) + n \sim O(n^2)$. Each 2-event group

in N_2 can form 3 different temporal relations, and thus, the total number of seasonal 2-event patterns is: $N_2 \times 3^1 \sim O(n^2 3^1)$. Similarly, the number of 3-event groups is: $N_3 = P(n, 3) + P(n, 2) + n \sim O(n^3)$, and the number of seasonal 3-event patterns is: $N_3 \times 3^3 \sim O(n^3 3^3)$. For mining h-event groups, the number of h-event groups is $O(n^h)$, while the number of seasonal h-event patterns is $O(n^h \times 3^{\frac{1}{2}h(h-1)}) \sim O(n^h 3^{h^2})$. Therefore, the total number of seasonal temporal patterns is $O(n) + O(n^2 3^1) + O(n^3 3^3) + \dots + O(n^h 3^{h^2}) \sim O(n^h 3^{h^2})$. \square

A.7 Lemma 4

Lemma 4. Let $S = \langle e_1, \dots, e_{n-1} \rangle$ be a temporal sequence that supports an $(n-1)$ -event pattern $P = \langle (r_{12}, E_{1 \rightarrow e_1}, E_{2 \rightarrow e_2}), \dots, (r_{(n-2)(n-1)}, E_{n-2 \rightarrow e_{n-2}}, E_{n-1 \rightarrow e_{n-1}}) \rangle$. Let e_n be a new event instance added to S to create the temporal sequence $S' = \langle e_1, \dots, e_n \rangle$.

The set of temporal relations \mathfrak{R} is transitive on S' : $\forall e_i \in S', i < n, \exists r \in \mathfrak{R}$ s.t. $r(E_{i \rightarrow e_i}, E_{n \rightarrow e_n})$ holds.

PROOF. Since $S' = \langle e_1, \dots, e_n \rangle$ is a temporal sequence, the event instances in S' are chronologically ordered by their start times. Then, $\forall e_i \in S', i \neq n: t_{s_i} \leq t_{s_n}$. We have:

- If $t_{e_i} \pm \epsilon \leq t_{s_n}$, then $E_{i \rightarrow e_i} \rightarrow E_{n \rightarrow e_n}$.
- If $(t_{s_i} \leq t_{s_n}) \wedge (t_{e_i} \pm \epsilon \geq t_{e_n})$, then $E_{i \rightarrow e_i} \supseteq E_{n \rightarrow e_n}$.
- If $(t_{s_i} < t_{s_n}) \wedge (t_{e_i} \pm \epsilon < t_{e_n}) \wedge (t_{e_i} - t_{s_n} \geq d_o \pm \epsilon)$ where d_o is the minimal overlapping duration, then $E_{i \rightarrow e_i} \not\cap E_{n \rightarrow e_n}$. \square

A.8 Lemma 5

Lemma 5. Let $N_{k-1} = (E_1, \dots, E_{k-1})$ be a candidate seasonal $(k-1)$ -event group, and E_k be a candidate seasonal single event. The group $N_k = N_{k-1} \cup E_k$ can form candidate seasonal k -event temporal patterns if $\forall E_i \in N_{k-1}, \exists r \in \mathfrak{R}$ s.t. $r(E_i, E_k)$ is a candidate seasonal temporal relation.

PROOF. Let p_k be any k -event pattern formed by N_k . Then p_k is a list of $\frac{1}{2}k(k-1)$ triples (E_i, r_{ij}, E_j) where each represents a relation $r(E_i, E_j)$ between two events. In order for p_k to be a candidate seasonal k -event temporal pattern, each of the relations in p_k must be a candidate seasonal temporal pattern (Def. 3.10, Eq. (2), and Lemmas 2 and 4). \square

A.9 Mining frequent seasonal k-event pattern

Complexity: Let n be the number of single events in HLH_1 , i be the average number of event instances of each event, r be the number of $(k-1)$ -event patterns in HLH_{k-1} , and u be the average number of granules of each event/temporal relation. The complexity of frequent seasonal k -event pattern mining is $O(n^2 i^2 u^2) + O(|F_1| \cdot |F_{k-1}| \cdot r \cdot k^2 \cdot u)$.

PROOF. * **The complexity of frequent seasonal 2-event pattern mining:** The Cartesian product of n events in HLH_1 generates n^2 2-event groups. Computing $maxSeason$ of n^2 2-event groups takes $O(n^2 u)$. For each 2-event group, we need to compute $maxSeason$ of their temporal relations, which takes $O(i^2 u^2)$. We have potentially n^2 nodes. And thus, it takes $O(n^2 i^2 u^2)$. For each candidate 2-event pattern, identifying the set of season \mathcal{PS}

takes $O(u)$. And we have potentially $(n^2 s)$ relations (s is the number of temporal relations). Thus, finding \mathcal{PS} takes $O(n^2 s u)$. The complexity of frequent seasonal 2-event pattern mining is: $O(n^2 u + n^2 i^2 u^2 + n^2 s u) \sim O(n^2 i^2 u^2)$.

* **The complexity of frequent seasonal k-event pattern mining ($k > 2$):** For each $(k-1)$ -event pattern, we need to compute the support set of $\frac{1}{2}(k-1)(k-2)$ triples, which takes $O(\frac{1}{2}(k-1)(k-2)u) \sim O(k^2 u)$. We have $|F_1| \times |F_{k-1}|$ events, each has r $(k-1)$ -event patterns. Thus, the complexity of computing $maxSeason$ is $O(|F_1| \cdot |F_{k-1}| \cdot r \cdot k^2 \cdot u)$. For each candidate pattern, identifying its \mathcal{PS} takes $O(u)$. We have potentially $|F_1| \times |F_{k-1}| \times r$ patterns. Thus, it takes $O(|F_1| \cdot |F_{k-1}| \cdot r \cdot u)$. The complexity of frequent seasonal k -event pattern mining ($k > 2$) is: $O(|F_1| \cdot |F_{k-1}| \cdot r \cdot k^2 \cdot u + |F_1| \cdot |F_{k-1}| \cdot r \cdot u) \sim O(|F_1| \cdot |F_{k-1}| \cdot r \cdot k^2 \cdot u)$.

Thus, the total complexity is $O(n^2 i^2 u^2) + O(|F_1| \cdot |F_{k-1}| \cdot r \cdot k^2 \cdot u)$. \square

A.10 Theorem

Theorem 1. (Lower bound of the maximum seasonal occurrence) Let μ be the MI threshold. If the NMI $\tilde{I}(X_S; Y_S) \geq \mu$, then the maximum seasonal occurrence of (X_1, Y_1) in \mathcal{D}_{SEQ} has a lower bound:

$$maxSeason(X_1, Y_1) \geq \frac{\lambda_2 \cdot |\mathcal{D}_{SEQ}|}{minDensity} \cdot e^{W\left(\frac{\log \lambda_1^{1-\mu} \cdot \ln 2}{\lambda_2}\right)} \quad (16)$$

where: $\lambda_1 = \min\{p(X_i), \forall X_i \in X_S\}$ is the minimum probability of $X_i \in X_S$, and $\lambda_2 = p(Y_1)$ is the probability of $Y_1 \in Y_S$, and W is the Lambert function [6].

PROOF. From Eq. (6), we have:

$$\tilde{I}(X_S; Y_S) = 1 - \frac{H(X_S | Y_S)}{H(X_S)} \geq \mu \quad (17)$$

Hence:

$$\frac{H(X_S | Y_S)}{H(X_S)} \leq 1 - \mu \quad (18)$$

First, we derive a lower bound for $\frac{H(X_S | Y_S)}{H(X_S)}$. We have:

$$\begin{aligned} \frac{H(X_S | Y_S)}{H(X_S)} &= \frac{p(X_1, Y_1) \cdot \log \frac{p(X_1, Y_1)}{p(Y_1)}}{\sum_i p(X_i) \cdot \log p(X_i)} \\ &+ \frac{\sum_{i \neq 1 \& j \neq 1} p(X_i, Y_j) \cdot \log \frac{p(X_i, Y_j)}{p(Y_j)}}{\sum_i p(X_i) \cdot \log p(X_i)} \end{aligned} \quad (19)$$

We first consider the numerator in Eq. (19), we have:

$$\begin{aligned} p(X_1, Y_1) \cdot \log \frac{p(X_1, Y_1)}{p(Y_1)} &+ \sum_{i \neq 1 \& j \neq 1} p(X_i, Y_j) \cdot \log \frac{p(X_i, Y_j)}{p(Y_j)} \\ &\leq p(X_1, Y_1) \cdot \log \frac{p(X_1, Y_1)}{p(Y_1)} \\ &\leq p(X_1, Y_1) \cdot \log \frac{p(X_1, Y_1)}{\lambda_2} \end{aligned} \quad (20)$$

where $\lambda_2 = p(Y_1)$.

Next, we consider the denominator in Eq. (19). Suppose that:

$$p(X_k) = \min\{p(X_i)\}, \forall X_i \in X_S \quad (21)$$

Then we have:

$$\begin{aligned}
p(X_i) &\geq p(X_k), \forall X_i \in X_S \\
&\Rightarrow \log p(X_i) \geq \log p(X_k) \\
&\Rightarrow p(X_i) \log p(X_i) \geq p(X_i) \log p(X_k) \\
&\Rightarrow \sum_i p(X_i) \log p(X_i) \geq \sum_i p(X_i) \log p(X_k) \\
&= \log p(X_k) \sum_i p(X_i) \\
&= \log p(X_k) \\
&= \log \lambda_1
\end{aligned} \tag{22}$$

where $\lambda_1 = p(X_k)$.

Replace Eqs. (20) and (22) into Eq. (19), we get:

$$\frac{H(\mathcal{X}_S | \mathcal{Y}_S)}{H(\mathcal{X}_S)} \geq \frac{p(X_1, Y_1) \cdot \log \frac{p(X_1, Y_1)}{\lambda_2}}{\log \lambda_1} \tag{23}$$

From Eqs. (18) and (23), it follows that:

$$\begin{aligned}
(1 - \mu) &\geq \frac{p(X_1, Y_1) \cdot \log \frac{p(X_1, Y_1)}{\lambda_2}}{\log \lambda_1} \\
&\Leftrightarrow p(X_1, Y_1) \cdot \log \frac{p(X_1, Y_1)}{\lambda_2} \geq \log \lambda_1^{1-\mu}
\end{aligned} \tag{24}$$

Assign $x = p(X_1, Y_1)$, $b = \log \lambda_1^{1-\mu}$. Replace x and b into Eq. (24), we get:

$$\begin{aligned}
x \cdot \log \frac{x}{\lambda_2} &\geq b \\
&\Leftrightarrow \frac{x}{\lambda_2} \cdot \log \frac{x}{\lambda_2} \geq \frac{b}{\lambda_2} \\
&\Leftrightarrow \frac{x}{\lambda_2} \cdot \frac{\ln \frac{x}{\lambda_2}}{\ln 2} \geq \frac{b}{\lambda_2} \\
&\Leftrightarrow \frac{x}{\lambda_2} \cdot \ln \frac{x}{\lambda_2} \geq \frac{b \cdot \ln 2}{\lambda_2}
\end{aligned} \tag{25}$$

Assign $y = \ln \frac{x}{\lambda_2} \Rightarrow \frac{x}{\lambda_2} = e^y$. Replace y and e^y into Eq. (25), we get:

$$\begin{aligned}
y \cdot e^y &\geq \frac{b \cdot \ln 2}{\lambda_2} \\
&\Leftrightarrow y \geq W\left(\frac{b \cdot \ln 2}{\lambda_2}\right), \text{ where } W \text{ is the Lambert function [6].} \\
&\Leftrightarrow \ln \frac{x}{\lambda_2} \geq W\left(\frac{\log \lambda_1^{1-\mu} \cdot \ln 2}{\lambda_2}\right) \\
&\Leftrightarrow e^{\ln \frac{x}{\lambda_2}} \geq e^{W\left(\frac{\log \lambda_1^{1-\mu} \cdot \ln 2}{\lambda_2}\right)} \\
&\Leftrightarrow \frac{x}{\lambda_2} \geq e^{W\left(\frac{\log \lambda_1^{1-\mu} \cdot \ln 2}{\lambda_2}\right)} \\
&\Leftrightarrow x \geq \lambda_2 \cdot e^{W\left(\frac{\log \lambda_1^{1-\mu} \cdot \ln 2}{\lambda_2}\right)} \\
&\Leftrightarrow p(X_1, Y_1) \geq \lambda_2 \cdot e^{W\left(\frac{\log \lambda_1^{1-\mu} \cdot \ln 2}{\lambda_2}\right)}
\end{aligned} \tag{26}$$

Since the relative support of (X_1, Y_1) in \mathcal{D}_{SEQ} is greater than or equal to the relative support of (X_1, Y_1) in \mathcal{D}_{SYB} [11], hence:

$$\frac{|SUP^{(X_1, Y_1)}|}{|\mathcal{D}_{\text{SEQ}}|} \geq \frac{|SUP_{\mathcal{D}_{\text{SYB}}}^{(X_1, Y_1)}|}{|\mathcal{D}_{\text{SYB}}|} = p(X_1, Y_1) \tag{27}$$

where $\frac{|SUP_{\mathcal{D}_{\text{SYB}}}^{(X_1, Y_1)}|}{|\mathcal{D}_{\text{SYB}}|}$ is the relative support of (X_1, Y_1) in \mathcal{D}_{SYB} . From Eqs. (26) and (27), it follows that:

$$\begin{aligned}
\frac{|SUP^{(X_1, Y_1)}|}{|\mathcal{D}_{\text{SEQ}}|} &\geq \lambda_2 \cdot e^{W\left(\frac{\log \lambda_1^{1-\mu} \cdot \ln 2}{\lambda_2}\right)} \\
&\Leftrightarrow \frac{|SUP^{(X_1, Y_1)}|}{\text{minDensity}} \geq \frac{\lambda_2 \cdot |\mathcal{D}_{\text{SEQ}}|}{\text{minDensity}} \cdot e^{W\left(\frac{\log \lambda_1^{1-\mu} \cdot \ln 2}{\lambda_2}\right)} \\
&\Leftrightarrow \text{maxSeason}(X_1, Y_1) \geq \frac{\lambda_2 \cdot |\mathcal{D}_{\text{SEQ}}|}{\text{minDensity}} \cdot e^{W\left(\frac{\log \lambda_1^{1-\mu} \cdot \ln 2}{\lambda_2}\right)}
\end{aligned} \tag{28}$$

We can derive a lower bound of μ from Eq. (28).

$$\begin{aligned}
\text{maxSeason}(X_1, Y_1) &\geq \frac{\lambda_2 \cdot |\mathcal{D}_{\text{SEQ}}|}{\text{minDensity}} \cdot e^{W\left(\frac{\log \lambda_1^{1-\mu} \cdot \ln 2}{\lambda_2}\right)} \geq \text{minSeason} \\
&\Rightarrow e^{W\left(\frac{\log \lambda_1^{1-\mu} \cdot \ln 2}{\lambda_2}\right)} \geq \frac{\text{minSeason} \cdot \text{minDensity}}{\lambda_2 \cdot |\mathcal{D}_{\text{SEQ}}|} \\
&\Leftrightarrow e^{W\left(\frac{\log \lambda_1^{1-\mu} \cdot \ln 2}{\lambda_2}\right)} \geq \rho
\end{aligned} \tag{29}$$

where $\rho = \frac{\text{minSeason} \cdot \text{minDensity}}{\lambda_2 \cdot |\mathcal{D}_{\text{SEQ}}|}$.

To solve Eq. (29), we consider two cases.

* **Case 1:** $0 \leq \rho \leq \frac{1}{e}$, we have:

$$\begin{aligned}
\frac{\log \lambda_1^{1-\mu} \cdot \ln 2}{\lambda_2} &\geq \frac{-1}{e} \\
&\Leftrightarrow \log \lambda_1^{1-\mu} \geq \frac{-\lambda_2}{e \cdot \ln 2} \\
&\Leftrightarrow (1 - \mu) \cdot \log \lambda_1 \geq \frac{-\lambda_2}{e \cdot \ln 2} \\
&\Leftrightarrow 1 - \mu \leq \frac{-\lambda_2}{e \cdot \ln 2 \cdot \log \lambda_1} \quad (\log \lambda_1 < 0) \\
&\Leftrightarrow \mu \geq 1 + \frac{\lambda_2}{e \cdot \ln 2 \cdot \log \lambda_1} \\
&\Leftrightarrow \mu \geq 1 - \frac{\lambda_2}{e \cdot \ln 2 \cdot \log \frac{1}{\lambda_1}}
\end{aligned} \tag{30}$$

* **Case 2:** $\rho > \frac{1}{e}$, we have:

$$\begin{aligned} \frac{\log \lambda_1^{1-\mu} \cdot \ln 2}{\lambda_2} &\geq \rho \cdot \log \rho \\ \Leftrightarrow \log \lambda_1^{1-\mu} &\geq \rho \cdot \lambda_2 \cdot \frac{\log \rho}{\ln 2} \\ \Leftrightarrow (1-\mu) \cdot \log \lambda_1 &\geq \rho \cdot \lambda_2 \cdot \frac{\log \rho}{\ln 2} \\ \Leftrightarrow 1-\mu &\leq \rho \cdot \lambda_2 \cdot \frac{\log \rho}{\ln 2 \cdot \log \lambda_1} \quad (\log \lambda_1 < 0) \\ \Leftrightarrow \mu &\geq 1 - \frac{\rho \cdot \lambda_2 \cdot \log \rho}{\ln 2 \cdot \log \lambda_1} \end{aligned} \quad (31)$$

□

B ADDITIONAL EXPERIMENTAL RESULTS

B.1 Baselines comparison

Figs. 19, 20, 21, and 22 show the experimental results on SC and HFM datasets.

As shown in Figs. 19 and 20, A-STPM achieves the best runtime among all methods, and E-STPM has better runtime than the baseline. The range and average speedups of A-STPM compared to other methods are: [1.4-3.1] and 2.2 (E-STPM), and [4.9-10.3] and 6.9 (APS-growth). The speedup of E-STPM compared to the baseline is [2.8-5.4] and 3.5 on average. Note that the time to compute MI and μ for SC and HFM in Figs. 19 and 20 are 0.9 and 1.2 seconds, respectively.

In terms of memory consumption, as shown in Figs. 21 and 22, A-STPM is the most efficient method, while E-STPM is more efficient than the baseline. The range and the average memory consumption of A-STPM compared to other methods are: [1.4-2.6] and 1.7 (E-STPM), and [2.5-6.3] and 3.7 (APS-growth). The memory usage of E-STPM compared to the baseline is [1.3-3.2] and 2.1 on average.

B.2 Scalability evaluation on synthetic datasets

Figs. 23 and 24 show the runtimes of A-STPM, E-STPM and the baseline when the number of sequences changes (y-axis is in log scale). We obtain the range and average speedups of A-STPM are: [1.4-2.7] and 2.1 (E-STPM), and [2.4-6.1] and 4.2 (APS-growth). Similarly, the range and average speedup of E-STPM compared to APS-growth is [1.6-3.5] and 2.8. We note that the baseline fails for larger configurations in this scalability study, i.e., on the synthetic SC at 60% sequences (Fig. 23a) and on the synthetic HFM at 100% sequences (Fig. 24a), showing that A-STPM and E-STPM can scale well on big datasets while the baseline cannot.

Figs. 25 and 26 compare the runtimes of A-STPM, E-STPM and APS-growth when changing the number of time series (y-axis is in log scale). We obtain the range and average speedups of A-STPM are: [1.4-2.9] and 2.2 (E-STPM), and [3.1-6.7] and 4.5 (APS-growth), and of E-STPM is [1.7-3.8] and 2.9 (APS-growth). The baseline also fails at large configurations in this study, i.e., when # Time Series ≥ 6000 on the synthetic SC (Fig. 25a) and the synthetic HFM (Fig. 26a).

Finally, we provide the percentage of time series and events pruned by A-STPM in the scalability test in Tables 10 and 11. Here, we can see that low *minSeason* and *minDensity* lead to more time

series (events) to be pruned because low *minSeason* and *minDensity* result in higher μ .

Table 10: Pruned Time Series and Events from A-STPM on SC

# Attr.	# Pruned Time Series			# Pruned Events		
	12-0.5%	16-0.75%	20-1.0%	12-0.5%	16-0.75%	20-1.0%
2000	31.60	29.20	25.30	30.23	26.26	20.04
4000	30.10	26.05	18.45	29.01	25.66	19.90
6000	28.35	24.22	18.25	28.83	25.02	19.83
8000	26.78	24.05	17.80	28.79	24.64	19.49
10000	26.03	23.01	17.49	25.19	22.53	18.13

Table 11: Pruned Time Series and Events from A-STPM on HFM

# Attr.	# Pruned Time Series			# Pruned Events		
	12-0.5%	16-0.75%	20-1.0%	12-0.5%	16-0.75%	20-1.0%
2000	38.10	31.35	28.90	27.46	24.68	20.72
4000	32.65	29.58	22.60	26.22	24.58	20.29
6000	31.12	27.85	20.28	25.41	23.78	19.84
8000	29.33	27.15	20.08	24.83	23.21	19.17
10000	28.84	25.09	19.68	24.54	23.01	18.97

B.3 Evaluation of the pruning techniques in E-STPM

In this section, we report the evaluation results of the proposed pruning techniques in E-STPM on SC and HFM. We use 3 different configurations that vary: the minimum season, the minimum density, and the maximum period. Figs. 27 and 28 show the results (the y-axis is in log scale). It can be seen that All-E-STPM achieves the best performance among all versions. Its speedup w.r.t. NoPrune-E-STPM ranges from 2.5 up to 4.5 depending on the configurations, showing that the proposed prunings are very effective in improving E-STPM performance. The average speedup is from 2 to 4 for Trans-E-STPM, and from 1.5 to 3 for Apriori-E-STPM. However, applying both always yields better speedup than applying either of them.

B.4 Evaluation of A-STPM

Table 12 shows the accuracies of A-STPM for different *minSeason* and *minDensity* on the real world datasets. It is seen that, A-STPM obtains high accuracy ($\geq 80\%$) when *minSeason* and *minDensity* are low, e.g., *minSeason* = 8 and *minDensity* = 0.5%, and very high accuracy ($\geq 95\%$) when *minSeason* and *minDensity* are high, e.g., *minSeason* = 16 and *minDensity* = 0.75%. Similarly, Table 13 shows the accuracies of A-STPM on the synthetic datasets: very high accuracy ($\geq 95\%$) when *minSeason* and *minDensity* are high, e.g., *minSeason* = 16 and *minDensity* = 0.75%.

Table 12: A-STPM Accuracy

# minSeason	minDensity (%)					
	SC (real)			HFM (real)		
	0.5	0.75	1	0.5	0.75	1
8	80	81	87	82	84	89
12	83	85	93	86	92	94
16	92	95	100	96	97	100
20	95	99	100	97	100	100

Table 13: The Accuracy of A-STPM on Syn. Data

# Attr.	SC			HFM		
	Accuracy (%)			Accuracy (%)		
	12-0.5%	16-0.75%	20-1.0%	12-0.5%	16-0.75%	20-1.0%
2000	84	95	100	87	98	100
4000	85	96	100	87	98	100
6000	85	97	100	90	98	100
8000	87	97	100	93	98	100
10000	88	98	100	94	99	100

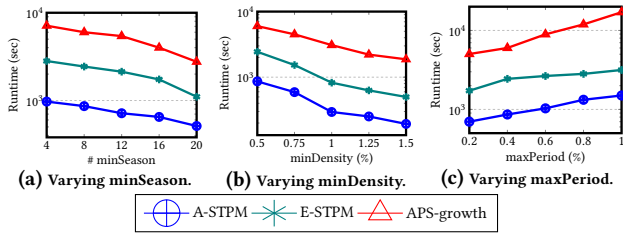


Figure 19: Runtime Comparison on SC (real-world)

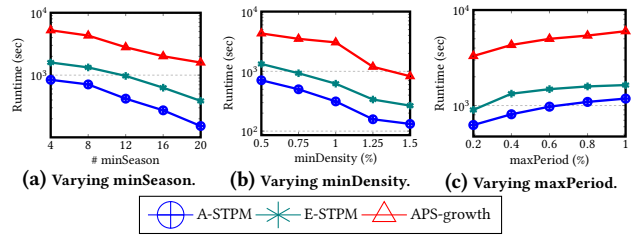


Figure 20: Runtime Comparison on HFM (real-world)

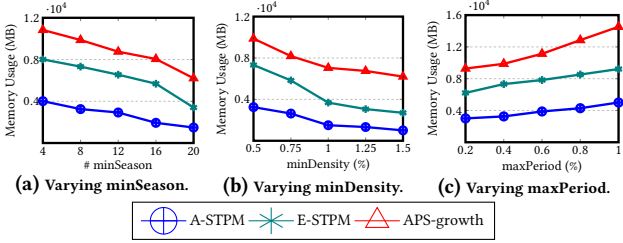


Figure 21: Memory Usage Comparison on SC (real-world)

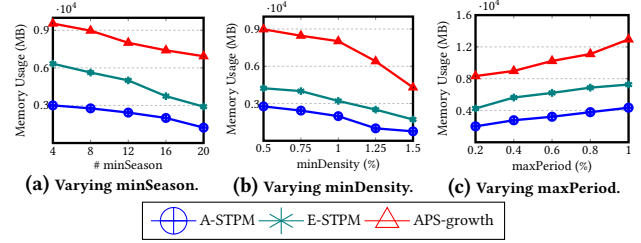


Figure 22: Memory Usage Comparison on HFM (real-world)

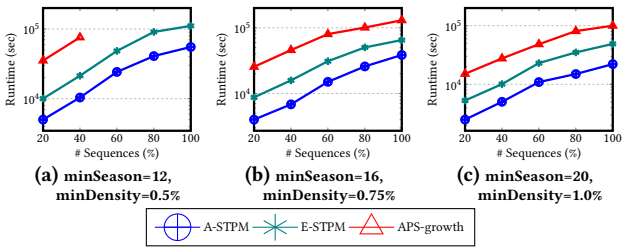


Figure 23: Scalability: Varying #Sequences on SC (synthetic)

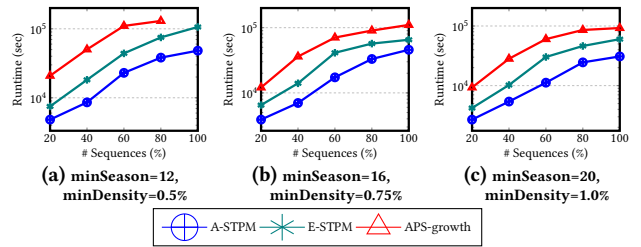


Figure 24: Scalability: Varying #Sequences on HFM (synthetic)

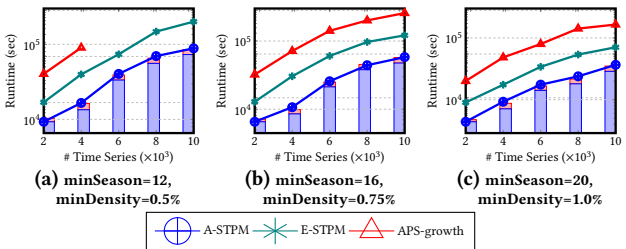


Figure 25: Scalability: Varying #TimeSeries on SC (synthetic)

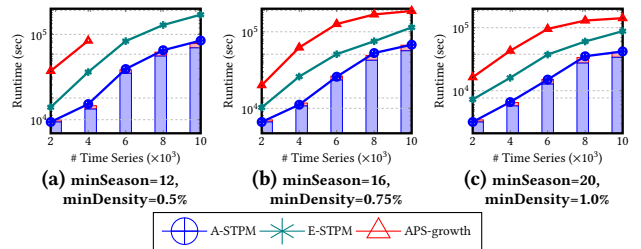


Figure 26: Scalability: Varying #TimeSeries on HFM (synthetic)

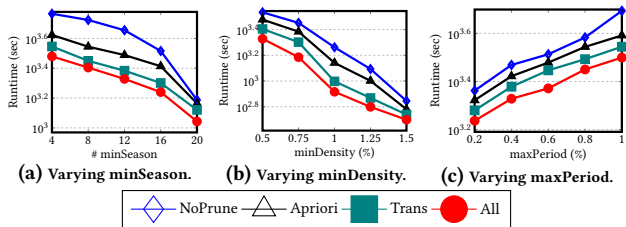


Figure 27: Pruning Techniques of E-STPM on SC (real-world)

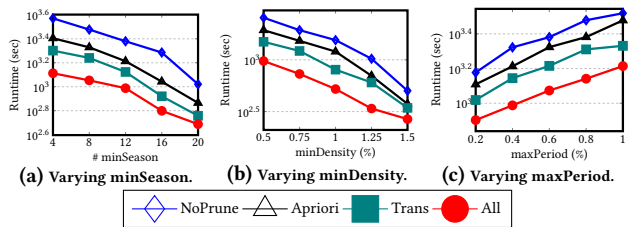


Figure 28: Pruning Techniques of E-STPM on HFM (real-world)

B.5 Evaluation of the tolerance buffer ϵ

We evaluate the impact of the buffer ϵ on extracted seasonal patterns. Tables 14 and 15 report the number of extracted seasonal patterns for different ϵ values, and the corresponding percentages of pattern loss compared to $\epsilon = 0$. For RE and SC datasets, there are no lost patterns with $\epsilon = 1$ hour. For INF and HFM datasets, there are no lost patterns with $\epsilon = 1$ day and $\epsilon = 2$ days. And the losses among other ϵ values are very low since there is low noise level in the datasets.

Table 14: Number of Extracted Patterns and Percentages of Pattern Loss on RE and SC

ϵ value	RE		SC	
	# Patterns	Patterns (%)	# Patterns	Patterns (%)
1 hour	19240	0.00	17241	0.00
2 hours	19139	0.52	16921	1.85
3 hours	19012	1.18	16812	2.48

Table 15: Number of Extracted Patterns and Percentages of Pattern Loss on INF and HFM

ϵ value	INF		HFM	
	# Patterns	Patterns (%)	# Patterns	Patterns (%)
1 day	7919	0.00	14763	0.00
2 days	7919	0.00	14763	0.00
3 days	7910	0.11	14750	0.08